

Retrofitting of Concrete-Encased Beam-Column Connection of an Historic Building using Fiber  
Reinforced Polymer

By Nitisha Parajuli, Bachelor of Engineering

A Thesis Submitted in Partial  
Fulfillment of the Requirements  
for the Degree of  
Master of Science  
in the Field of Civil Engineering

Advisory Committee:

Brad Cross, Chair

Nader Panahshahi

Jianwei Huang

Graduate School  
Southern Illinois University Edwardsville  
May 2019

ProQuest Number: 13877686

All rights reserved

INFORMATION TO ALL USERS

The quality of this reproduction is dependent upon the quality of the copy submitted.

In the unlikely event that the author did not send a complete manuscript and there are missing pages, these will be noted. Also, if material had to be removed, a note will indicate the deletion.



ProQuest 13877686

Published by ProQuest LLC (2019). Copyright of the Dissertation is held by the Author.

All rights reserved.

This work is protected against unauthorized copying under Title 17, United States Code  
Microform Edition © ProQuest LLC.

ProQuest LLC.  
789 East Eisenhower Parkway  
P.O. Box 1346  
Ann Arbor, MI 48106 – 1346

## ABSTRACT

### RETROFITTING OF CONCRETE-ENCASED BEAM-COLUMN CONNECTION OF AN OLD HISTORIC BUILDING USING FIBER REINFORCED POLYMER

by

NITISHA PARAJULI

Chairperson: Professor Brad Cross

With the increasing demand for rehabilitation of historic structures, much research has been completed on retrofitting techniques of old steel frame buildings. Many existing buildings in the United States are concrete-encased steel frame buildings designed in the early 1900s for the advantages they provide such as resistance to fire and corrosion. With age, these types of old buildings have lost their strength and need attention to function efficiently for future uses. This research has focused on nonlinear finite element analysis of a connection of an old historic building, the Syndicate Building in St. Louis, MO, to investigate the improvement in structural performance of concrete-encased steel beam-column connection. Finite element analysis is an economical tool which is used in this study to predict the moment-rotation ( $M-\theta$ ) relationship and load-deformation relationship of the joint before and after the application of the FRP confinement. The FRP retrofitted connection showed improvement in the load carrying capacity and moment capacity of the riveted beam-column connection compared to the plain concrete-encased model.

@Copyright by Nitisha Parajuli May 2019  
All Rights Reserved

## ACKNOWLEDGEMENT

Firstly, I would like to express my sincere gratitude to Prof. Brad Cross, Ph.D., S.E., for providing me guidance and continuous support throughout my research. His suggestions and directions have helped me overcome complicated issues during the research. He has also given his time to review my writing and helped me prepare this final thesis. It was a great opportunity to be able to work on this research topic individually and independently. I would also like to express my appreciation to my advisory committee members, Dr. Nader Panahshahi and Dr. Jianwei Huang.

Secondly, I am thankful to Mr. Joe Carpenter from KPFF for his genuine contribution towards providing the resources for the research. He has made available the original construction drawings of the building named *The Syndicate* whose section was analyzed in this project. I really appreciate his effort to donate a sample section of a similar connection for experimental purposes to the Department of Civil Engineering, SIUE.

Last but not the least a big thank you goes to my friends and family who have always loved and encouraged me through every step of my life.

## TABLE OF CONTENTS

ABSTRACT .....	ii
ACKNOWLEDGEMENT.....	iii
LIST OF FIGURES .....	vi
LIST OF TABLES .....	ix
CHAPTER I. INTRODUCTION.....	1
1.1. Background.....	1
1.2. Motivation .....	2
1.3. Statement of Problem.....	3
1.4. Organization of Thesis .....	4
CHAPTER II. LITERATURE REVIEW .....	7
2.1. General .....	7
2.2. Methods of Retrofitting.....	7
2.3. Experimental Investigations .....	9
2.3.1. Tests of Reinforced Concrete Connections .....	9
2.3.2. Tests of Bare Steel Connections .....	16
2.3.3. Tests of Concrete-Encased Steel Connections .....	17
2.4. Analytical Investigation (Finite Element Analysis).....	18
2.4.1. Study of Reinforced Concrete Beam and Column .....	18
2.4.2. Study of Riveted Connections .....	19
CHAPTER III. FINITE ELEMENT ANALYSIS .....	25
3.1. Finite Element Analysis of Behavior of Riveted Lap Joint.....	25
3.1.1. Geometry and Material of Riveted Lap Joints .....	25
3.1.2. Finite Element Analysis of the Lap Joint .....	26
3.1.3. Analysis Results.....	28
3.2. Finite Element Analysis of Steel Column with Concrete-Filled Composite Jackets .....	30

3.2.1.	Geometry and Material Properties .....	30
3.2.2.	Finite Element Analysis of Composite Column .....	34
3.2.3.	Analysis Results.....	35
CHAPTER IV. ANALYSIS OF CONCRETE-ENCASED BEAM-COLUMN CONNECTION		39
4.1.	Introduction to the Syndicate Building .....	39
4.2.	General Description of Beam-Column Joint of the Syndicate Building.....	39
4.3.	Finite Element Analysis of Beam-Column Connection.....	45
4.4.	Finite Element Analysis of Concrete-Encased Beam Column Connection .....	46
4.4.1.	Description of Finite Element Model of Bare Steel Connection.....	46
4.4.2.	Geometry and Material Properties .....	49
4.4.3.	Finite Element Idealization of the Connection .....	51
4.4.4.	Analysis Results.....	53
4.5.	Finite Element Modeling of Behavior of Retrofitted Concrete-Encased Connection ....	56
4.5.1.	Geometry and Material Properties .....	57
4.5.2.	Finite Element Idealization of the model .....	59
4.5.3.	Analysis Results.....	59
CHAPTER V. COMPARISON AND DISCUSSION OF RESULTS.....		65
5.1.	Comparison of Retrofitted and Non-Retrofitted Connection.....	65
5.2.	Problems Encountered and Limitations .....	75
5.3.	Future Work.....	76
CHAPTER VI. CONCLUSION .....		77
REFERENCES .....		79

## LIST OF FIGURES

Figure 1. Details of FRP sheets and wraps for beam, column and slab strengthening (Drawing provided by FYFE) .....	5
Figure 2. Concrete jacketing (Wu et al. 2006).....	8
Figure 3. Steel jacketing (Wu et al. 2006).....	8
Figure 4. Other types of jacketing: (a) FRP jacketing; (b) Hybrid jacketing (Wu et al. 2006).....	9
Figure 5. Configuration of FRP retrofitting in a specimen (Azarm et al. 2016) .....	10
Figure 6. Final crack pattern for (a) control specimen; (b) retrofitted specimen (Azarm et al. 2016).....	10
Figure 7. (a) CFRP retrofitting scheme; (b) Failure mode in retrofitted specimen .....	11
Figure 8. (a) CFRP Lap splice technique; (b) CFRP sheet at bottom surface of beam; (c) CFRP shear reinforcement; (d) CFRP column confinement (Pantelides et al. 2008) .....	13
Figure 9. Different types of FRP orientation (Le-Trung et al. 2009).....	14
Figure 10. Diagonal wrapping and anchored U shaped GFRP (Ghobarah et al 2001).....	15
Figure 11. Failure modes of different specimen with FRP confinement (Karimi et al. 2009).....	16
Figure 12. T-stub joint: rupture point under shear load (Naderi 2008).....	20
Figure 13. (a) Flexural yielding; (b) shear yielding; in clip angle joint under tension load (Naderi 2008).....	20
Figure 14. (a) FE model of multiple riveted connection; (b) Crack configuration (Rodrigues et al. 2010) .....	21
Figure 15. FE meshing of double-lap riveted joint (Imam et al. 2007) .....	22
Figure 16. (a) Possible crack initiation pattern; (b) Fatigue crack initiation hot spots on holes ...	22
Figure 17. Lap joint with five rivets before and after failure (Pavan et al. 2011) .....	23
Figure 18. Normalized load-deformation curve for riveted joint, experimental (Pavan et al. 2011).....	24
Figure 19. Geometry of single row five-rivet lap joint .....	26
Figure 20. Stress-strain relationship used for plates (Pavan et al., 2011) .....	27



Figure 21. ANSYS finite element mesh for riveted lap joint .....	28
Figure 22. Normalized load versus deformation (Experimental by Pavan et. al and ANSYS).....	29
Figure 23. Geometry of composite column .....	31
Figure 24. Material properties for steel model .....	31
Figure 25. Linear material properties for concrete model.....	32
Figure 26. Stress-strain graph of concrete used in ANSYS according to MacGregor (1992). ....	33
Figure 27. Orthotropic elasticity property of CFRP in Y-direction.....	34
Figure 28. Finite Element Meshing of the Composite Column.....	35
Figure 29. Axial Load-displacement curve of the control specimen (Karimi et al. 2011).....	36
Figure 30. Stress-strain relationship for (a) steel; (b) confined concrete; used in the analytical study (Karimi et al. 2011).....	37
Figure 31. Axial Load-Displacement Curve obtained from ANSYS FEA vs. Experiment .....	38
Figure 32. The Syndicate Trust Building (Original building drawing provided by KPFF) .....	40
Figure 33. Floor elevation of the building (Original building drawing provided by KPFF) .....	40
Figure 34. Ground floor plan of the building (Original building drawing provided by KPFF) ....	41
Figure 35. Typical beam-column section (Original building drawing provided by KPFF).....	42
Figure 36. Cross-section detail of steel beam-column connection .....	43
Figure 37. Cross-section of built-up column .....	43
Figure 38. Typical cross-section of (a) Z-section; (b) I-section; (c) Plan of L-section; .....	44
Figure 39. Typical section of concrete-encased connection.....	45
Figure 40. Material properties for rivet model .....	47
Figure 41. Material properties for steel plate model.....	47
Figure 42. Material property for structural steel model .....	48
Figure 43. Closer view of riveted connection of the joint.....	48
Figure 44. ANSYS model of beam-column connection .....	49
Figure 45. Linear material property for concrete model of C1 specimen .....	50

Figure 46. Stress-strain graph of concrete of C1 specimen used in ANSYS according to MacGregor (1992).....	51
Figure 47. ANSYS model (Concrete-encased beam-column connection).....	52
Figure 48. Meshed model (Concrete-encased beam-column connection) .....	53
Figure 49. Load-displacement graph of concrete-encased control specimens .....	54
Figure 50. Moment-rotation curve of concrete-encased models .....	55
Figure 51. Cross-section details of retrofitted connection (T1 specimen) .....	57
Figure 52. Orthotropic elasticity material property of FRP .....	58
Figure 53. ANSYS model of retrofitted concrete-encased beam-column connection.....	60
Figure 54. Meshed Model of Retrofitted Beam-column connection .....	61
Figure 55. Deformed Shape of Retrofitted Model T3 (loading in +Z direction).....	62
Figure 56. Load-displacement curve of retrofitted specimens T1, T2 and T3 .....	63
Figure 57. Moment-rotation curve of retrofitted models T1, T2 and T3 .....	64
Figure 58. Maximum principal stress in; (a) C1 specimen; (b) T1 specimen; (c) T2 specimen ...	68
Figure 59. Comparison of load displacement graph (Non-retrofitted v/s retrofitted) using 2ksi concrete .....	69
Figure 60. Comparison of moment rotation curve for plain and retrofitted specimens with 2ksi concrete .....	70
Figure 61. Comparison of load deformation curve for plain and retrofitted specimens .....	71
Figure 62. Comparison of moment rotation curve for plain and retrofitted specimens .....	72
Figure 63. Maximum principal stress in; (a) C1 specimen; (b) T1 specimen; (c) T2 specimen ...	73

## LIST OF TABLES

Table 1. Material Properties of Elements Used in FE Analysis .....	26
Table 2. Material Properties of FRP .....	33
Table 3. Material Properties of Steel (ASCE 41-17) .....	46
Table 4. Material Properties of Concrete .....	50
Table 5. Description of Models used in Finite Element Analysis .....	56
Table 6. Material Properties of FRP (obtained from FYFE catalogue) .....	58
Table 7. Finite Element Analysis Result for Retrofitted Specimen .....	61
Table 8. Comparison of Plain and Retrofitted Model Capacity .....	67

## CHAPTER I. INTRODUCTION

### 1.1. Background

Concrete-encased steel frames have been used in engineering practice for many years. Engineers started using steel shapes encased in concrete since the 1930s for the advantages they provide such as resistance to fire and corrosion. In more recent times, composite frame construction gained popularity in the 1960s and it developed as a common and viable structural member type (*Steel Design Guide 6, 1992*). A building that is comprised of a concrete-encased steel column with structural steel and a concrete deck makes up a composite frame system. Composite frame construction can be found in many structures worldwide.

The most important reason for encouraging composite construction is that the two components such as structural steel and reinforced concrete in association produce a composite structure having the advantages of each material (*Steel Design Guide 6, 1992*). Composite frame construction has various advantages such as smaller cross sections, large load carrying capacity, ductility in earthquake zones, speed in erection of frame, inherent stiffness due to reinforced concrete that controls the building drift, light weight, strength, fire resistance and high damping characteristics. However, composite columns also show disadvantages like creep and column shortening.

More recently, concrete-encased steel frame buildings are used in many high-rise structures owing to the strengthening and stiffening benefits of concrete on capacity enhancement of the encased steel. Historic buildings that were constructed in the early 1900s have aged and diminished their original functions. Therefore, it is essential to upgrade existing structures for future use. An “adaptive reuse” is a concept of strengthening these original structures for new modern day uses.

It is an economical process with which an old building can be transformed into a building with vibrant facilities bypassing the inefficient process of demolition and reconstruction of huge buildings. This report has discussed the need to retrofit the structures and different types of measures and materials that can be added to the existing structure to enhance their capacity.

## 1.2. Motivation

Many historic buildings in the United States are concrete-encased steel frame buildings designed and built in the early 1900s. The core purpose of using concrete encasement in that era was to protect the structure against fire and steel corrosion. However, concrete confinement not only made the steel fire and corrosion resistant but also added strength. With age, these kinds of old buildings have lost their strength and need efforts to function efficiently for future purposes. Today, preservation of existing buildings has explored the concept of “Sustainability begins with Preservation”. According to Rocchi (2015) the preservation of historic buildings has grown in importance due to the following reasons:

- Some buildings are built with higher quality and rare materials which no longer exist.
- Economic advantages for certain type of businesses when located in older buildings.
- Attraction of people towards old buildings.
- Old buildings are the reminder of city’s culture and complexity.
- Economic saving of cost of demolition and reconstruction of every old building.

### 1.3. Statement of Problem

The demand of rehabilitation of historic old buildings to make them reusable in a more affordable way seems to be high. Dozens of cities throughout the United States have high rise steel framed construction from the early 1900s, and it is uneconomical to demolish and reconstruct all the existing old high-rise buildings for future use. This limitation has intrigued the interest of many researchers to find a way to include the latest technology in existing buildings to meet the current building code requirements. There has been an extensive amount of research on retrofitting of existing structures. Some different types of techniques used so far are steel, concrete and fiber reinforced polymer (FRP) jacketing. The use of concrete jacketing and steel jacketing for retrofitting of structures has shown significant increase in overall stiffness of the structure. The increased stiffness of the retrofitted system is likely to attract more seismic load which is not desired. Thus, FRP wraps for retrofitting have become more popular.

Fiber reinforced polymer (FRP), which is also known as fiber reinforced plastic, is a composite material made up of polymer matrix reinforced with fibers such as glass, carbon or aramid (Masuelli, 2013). FRPs are stiff, durable, lightweight and non-toxic, which has made it attractive to structural engineers. Many researchers have concluded that using an externally bonded FRP wrap has showed enhancement in the axial load carrying capacity of columns and the bending capacity of beams. It also showed an increased strength of the structure against special loads like earthquake and impact. This thesis will study and analyze the effect of externally bonded FRP sheets to improve the capacity of the beam-column connection.

A beam, column, slab strengthening drawing produced by the FYFE in 2005 is taken as a reference for the configuration of FRP sheets for the analysis. The drawing was produced for a concrete-

encased steel beam-column joint and is provided in Figure 1 (and described in more detail in Chapter 4). A beam-column connection of an old historic landmark building in downtown St. Louis, The Syndicate Trust Building, built in 1907 is considered for research on increasing the capacity of the connection using FRP. The main objective of this thesis is to test the efficiency of the FYFE drawing in enhancing the capacity of the connection using finite element analysis in finite element software ANSYS 17.2.

#### 1.4. Organization of Thesis

The thesis has been divided into four chapters. The chapters are described briefly as follows:

**Chapter 1** introduces concrete-encased steel frame construction, its benefits and disadvantages of use in the old buildings. It presents the history of use of these frame constructions and the development of the technology with time. This chapter also discusses the motivation, need to retrofit historic structures and the scope of the thesis.

**Chapter 2** discusses the previous research and experimental studies that have been performed in retrofitting or strengthening of old historic buildings throughout the world. In this chapter, retrofitting measures adopted to strengthen reinforced concrete and bare steel beam-column connections have been presented with the results obtained. It also presents studies on riveted connections and their finite element (FE) modeling requirements.

**Chapter 3** introduces the finite element analysis (FEA) of the two models considered to validate the modeling requirement in the software ANSYS. This section incorporates the geometry, material properties, boundary conditions, finite element idealization and discusses the results obtained from two different models used in the previous research discussed in Chapter 2.





**Chapter 4** introduces the Syndicate Building and its structural features and describes the details of the beam-column connection that is used in the building. The behavior of the joint before and after the application of FRPs is analyzed using an ANSYS finite element analysis. This section discusses in detail the geometry, material properties, boundary conditions and finite element idealization of the model of the connection.

**Chapter 5** provides the conclusions and recommendations of the work done during the thesis.

## CHAPTER II. LITERATURE REVIEW

### 2.1. General

Many existing buildings were designed and constructed before the time when seismic codes or ductile reinforcement detailing codes were developed. Most of these structures are designed as conventional weak column/strong beam system. These old buildings might meet the past standard for strength but lack the ductility required in current codes. Inadequate reinforcement in the joints have caused many joint failures during earthquakes. Thus, it has become vital to retrofit these structures to maintain a safer infrastructure and come up with economical methods to enhance the capacity of beam-column joints to protect them from future earthquakes.

The connections in old steel frame systems (pre-1976 buildings) were typically made of semi-rigid riveted or bolted connections (Shanmuganathan and Clifton 2004). Shanmuganathan and Clifton (2004) evaluated the seismic resistance of old moment resisting steel frame systems and determined that the joint connections in these structures are critical in terms of strength and rotation capacity. The poor performance of such old structures was related to lack of provision for adequate load transfer through connection to the vertical load carrying members.

### 2.2. Methods of Retrofitting

Wu et al. (2006) reviewed hundreds of papers and analyzed more than 700 reinforced concrete (RC) column tests to identify different retrofitting techniques that can be adopted. The paper discusses concrete jacketing, steel jacketing and fiber reinforced polymer (FRP) jacketing, as shown in Figure 2, Figure 3 and Figure 4, respectively, as an effective method to enhance flexural

and shear strength of a column. However, concrete and steel jacketing can significantly increase the stiffness of the structural system and attract more seismic load. Partial interaction plating is another unique technique in which steel plates are bolted to specific locations such as tension and/or compression faces to improve the resistance of those faces of the column without increasing whole column stiffness. Their investigation concluded that adequate and sufficient confinement of jacketing is key for effective retrofitting. Recently, FRP has developed interest among many researchers to improve the strength of beam-column connections.

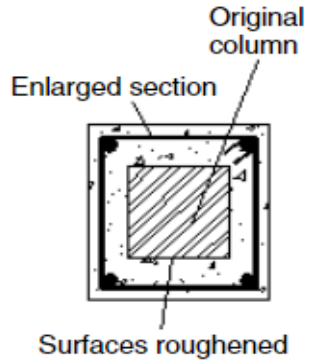


Figure 2. Concrete jacketing (Wu et al. 2006)

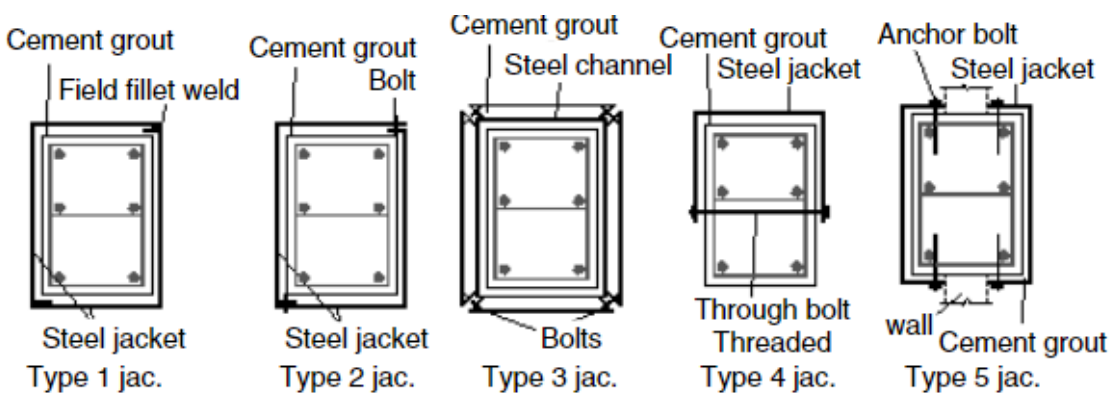


Figure 3. Steel jacketing (Wu et al. 2006)

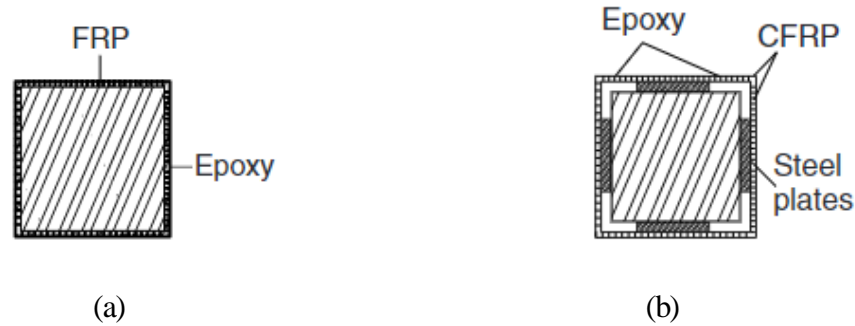


Figure 4. Other types of jacketing: (a) FRP jacketing; (b) Hybrid jacketing (Wu et al. 2006)

### 2.3. Experimental Investigations

It is essential to investigate the experimental data obtained from different researchers to understand the behavior of the connections and also it serves as a basis for a reliable validation of the analytical methods that are adopted in the analysis. FRP retrofitting technique has been adopted in a broad variety of connections to evaluate the performance.

#### 2.3.1. *Tests of Reinforced Concrete Connections*

In an experimental study, Azarm et al. (2016) tested two full scale RC beam-column joints with FRP laminates placed on the top and bottom of beam ends joining the joints and CFRP sheets at certain distance from column face to check the performance of joints. The configuration of the FRP laminate is shown in Figure 5. The flange bonded retrofitting resulted in an increase in the strength capacity of the joint by 23%. Also, the plastic hinge was relocated away from the column face, as seen in Figure 6, when the thickness of overlay was increased.

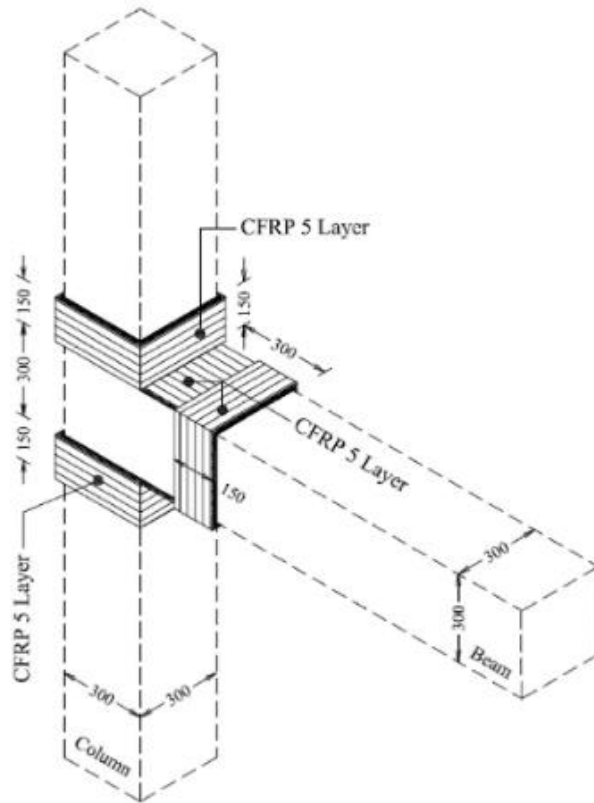


Figure 5. Configuration of FRP retrofitting in a specimen (Azarm et al. 2016)

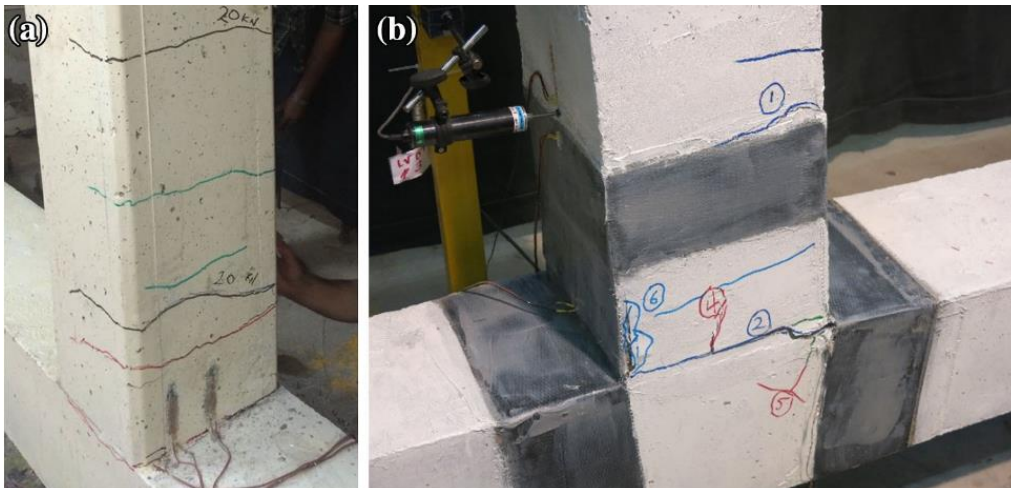


Figure 6. Final crack pattern for (a) control specimen; (b) retrofitted specimen (Azarm et al. 2016)

Mostofinejad et al. (2017) performed a numerical and experimental study on FRP composites in beam-column connections. Their study attempts to estimate the strength and displacement of the connection up to the failure point. A unidirectional Carbon Fiber Reinforced Polymer (CFRP) composite wrap was provided to the top and bottom of the column and CFRP sheets were applied at the top and bottom side of the beam longitudinally along the direction of reinforcement. The sheets were inserted into a groove prepared at the concrete cover to provide adequate anchorage as shown in Figure 7 (a). CFRP wrap was also provided to prevent de-bonding failure. The results obtained showed significant improvement in loading capacity of the beam-column connection, however, a decrease of displacement capacity and energy dissipation of the connection was obtained. It was also obtained that only one layer of CFRP sheet is needed to shift the location of plastic hinge away from the beam column interface [Figure 7 (b)]. The failure in the retrofitted specimen was obtained at the beam at cutoff point of CFRP sheets.

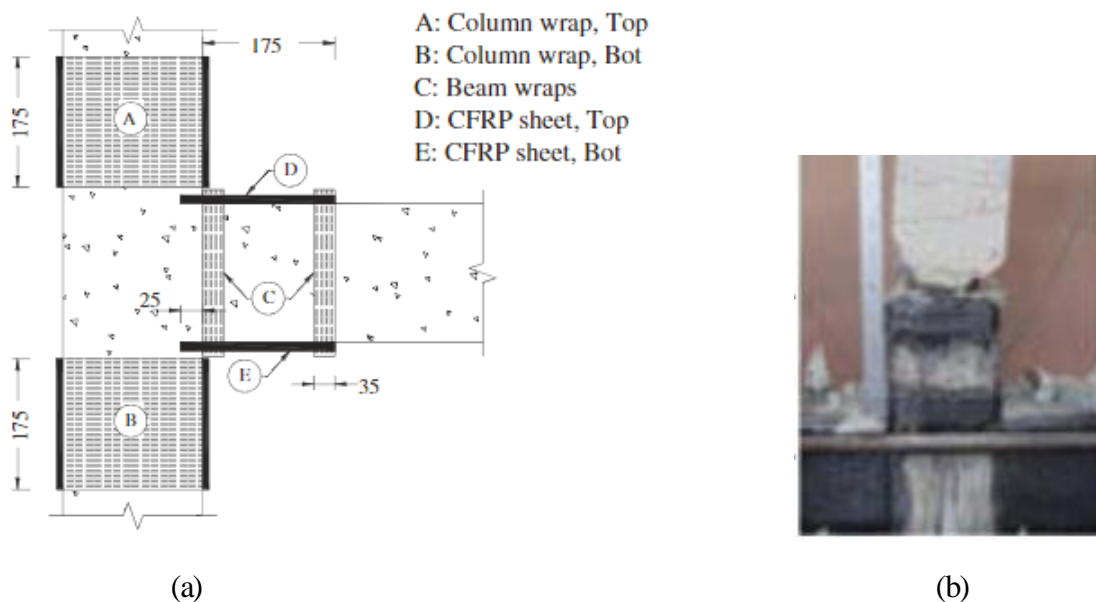


Figure 7. (a) CFRP retrofitting scheme; (b) Failure mode in retrofitted specimen  
(Mostofinejad et al. 2017)

From an experimental study to upgrade the behavior of a RC beam column connection, Hosseini et al. (2018) suggested the use of engineered cementitious composite (ECC) to improve the capacity and damage tolerance of the beam-column connection. A high-performance fiber reinforced cementitious composite (HPFRCC) was used in specific zones such as joint panels and potential plastic hinge regions only to record the performance enhancement of the connection. Due to its high cost, it is only used in potential plastic hinge regions. Qudah and Maalej (2014) also investigated the application of ECC in beam-column connection and came to report that ECC can increase the energy absorption capacity of the joint up to 20%.

Pantelides et al. (2008) did an experimental study on a beam-column connection joints using CFRP composite laminates to improve the shear capacity, ductility, energy dissipation and rotational capacity of the joint. An external CFRP lap splice was used to improve the bond of the bottom steel reinforcement of the beam as shown in Figure 8(a). Their calculation showed that the CFRP lap splice is able to carry tension force in the bottom reinforcement from one end of the joint to other. In another investigation, a CFRP composite sheet was applied at the bottom of the beam surface (Figure 8(b)), to postpone the growth of flexure and shear crack. They also provided two layers of CFRP U stirrups, placed in the region as shown in Figure 8(c) to minimize the shear failure and CFRP confinement of column as shown in Figure 8(d). The experimental result showed increase in the stiffness of the rehabilitated specimen due to additional reinforcement by CFRP composites. However, the energy dissipation was about 2.3 times than that of as-built specimen, demonstrating improvement in performance in flexure and in shear. It was also concluded that CFRP delamination was the initiating cause of failure, as bulging failure mechanism i.e. fracture of concrete was developed inside the joint.

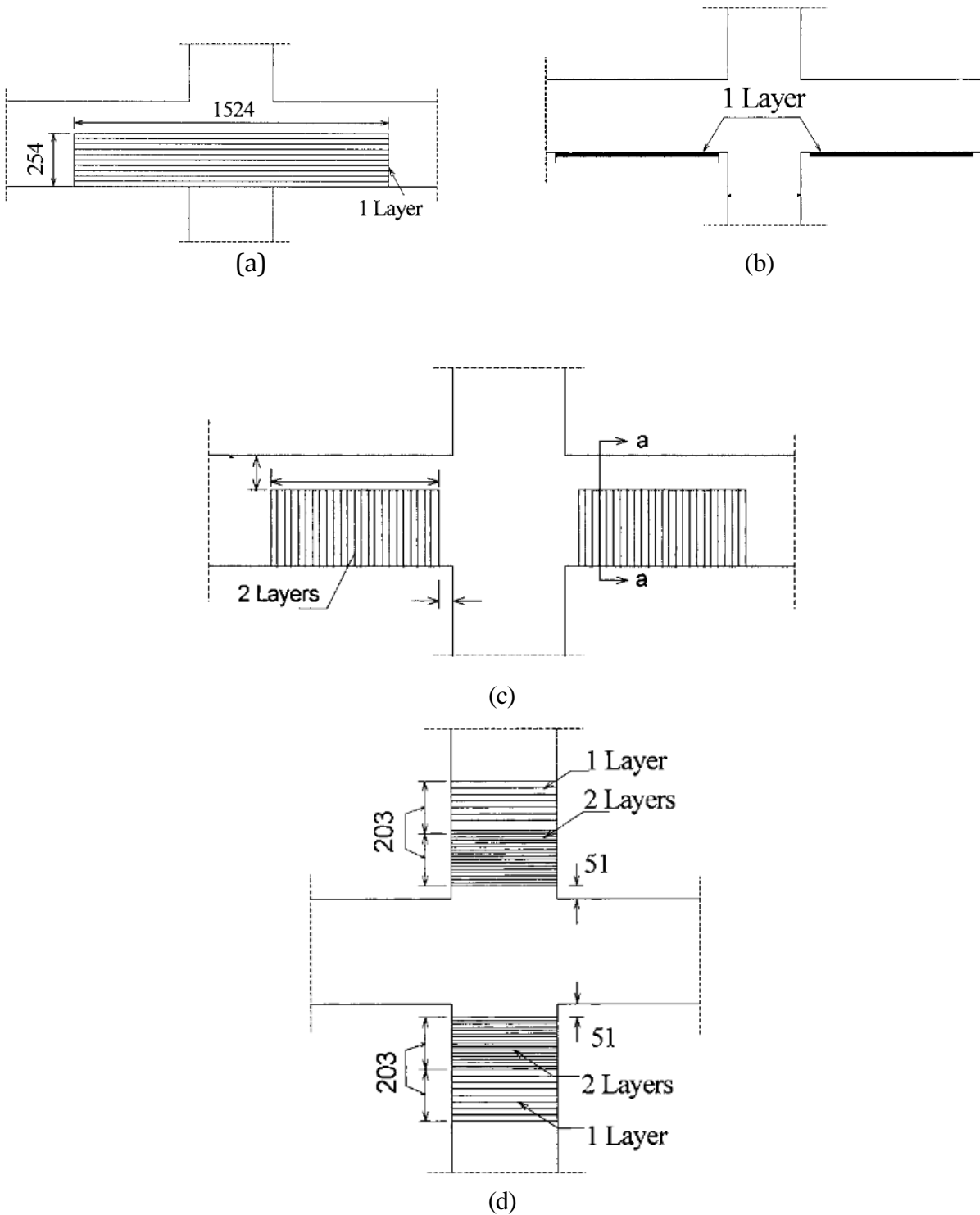


Figure 8. (a) CFRP Lap splice technique; (b) CFRP sheet at bottom surface of beam; (c) CFRP shear reinforcement; (d) CFRP column confinement (Pantelides et al. 2008)



Several orientations of CFRP sheets were studied by Le-Trung et al. (2009) to find out the most effective method of applying CFRP sheets to improve the seismic performance of the joints. Different shapes considered were T-shape, X-shape, L-shape and strip combination as shown in Figure 9. The test results showed that the direction of CFRP fibers which are similar to the direction of the principal stresses has significant influence in enhancing the strength and ductility of the joint. Their result showed that three particular configurations which are X-shaped wrapping, application of strips on the column and wrapping of two layers of CFRP sheets showed better performance in terms of ductility and strength than other configurations.

Ghobarah et al. (1997) attempted to rehabilitate lap splices in columns using flat steel sheets as jackets in reinforced concrete column that caused bulging problems. They proposed to use anchors to prevent the bulging problem. In another attempt, Ghobarah et al. (1997) investigated corrugated steel jackets as confinement that showed positive response in terms of upgrading shear strength as well as control of bulging problems.

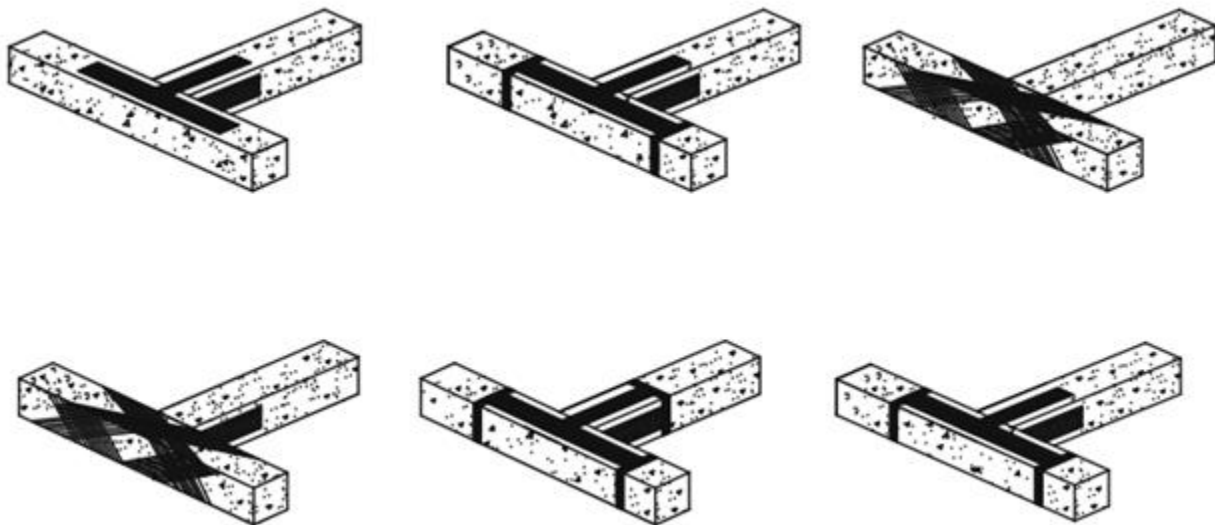


Figure 9. Different types of FRP orientation (Le-Trung et al. 2009)

Ghobarah et al. (2001) aimed to increase the shear strength of the joint by shifting the failure to beam flexural hinging mechanism to prevent brittle shear failure. In this paper, they investigated use of glass fiber reinforced polymer (GFRP) to improve ductile behavior of the joint. Four RCC beam-column joints representing pre-1970 construction was replicated and tested using constant axial column load and quasi-static cyclic load test. The first scheme where GFRP was wrapped in shape of “U” around the joint did not contribute much to strengthen the shear capacity and delamination of FRP occurred. GFRP “U” shaped wrap tied together using steel plates was another scheme that showed partial de-bonding of FRPs, but the plastic hinge was relocated away from the face of the column, in the beam, at the distance approximately equal to the depth of the beam. Two layers of “U” anchored GFRP fabric extended above and below the joint wrapped around the column performed well without de-bonding, shear cracking and triggering failure due to flexural hinge in beam. The last test specimen with three layers of unidirectional GFRP wrapped in diagonal 45 degrees in the joint delayed the shear failure by initiating flexural plastic hinge formation in the beam at the face of column. The paper focused on the fact that less than adequate confinement can delay shear failure but not prevent it. The application of the FRP wrap is shown in Figure 10.



Figure 10. Diagonal wrapping and anchored U shaped GFRP (Ghobarah et al 2001)

### 2.3.2. Tests of Bare Steel Connections

Traditional retrofitting methods for steel columns included either concrete-encased steel columns or concrete filled steel tubular columns (Karimi et al., 2009). There has been very limited research on strengthening of steel beams and columns using FRP composites due to lack of connection details. Karimi et al. (2009) investigated the performance of steel column wrapped with FRP and the void formed between them was filled with concrete. The specimen was wrapped with a single GFRP layer and an additional layer of CFRP. They performed both experimental test and analytical finite element (FE) test to find that the ultimate strength of retrofitted columns was two to three times greater than the control steel specimen. It was also observed that an upgrade in the ultimate strength was linearly increasing with the number of CFRP wraps, however with increasing number of wraps, the section showed more brittle behavior. The mode of failures obtained in their experimental study is shown in Figure 11.

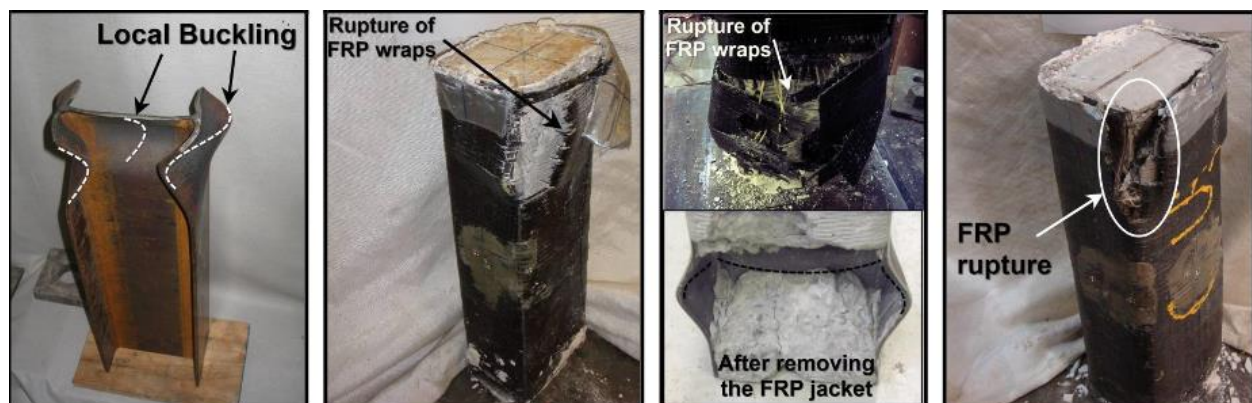


Figure 11. Failure modes of different specimen with FRP confinement (Karimi et al. 2009)

In another experimental study, Karimi et al. (2011) investigated steel column strengthening using wet lay-up fiber-reinforced polymer. The columns were wrapped with epoxy saturated FRP sheets and the void between them was filled with concrete. They reported that FRP confinement provided a significant increase in the ultimate capacity of the composite column with the increase of number of wraps. However, with the enhancement in energy dissipation characteristics, the composite column was also inclined more towards brittle failure than in unstrengthened steel columns, due to the brittle nature of concrete and FRP. In this paper, an analytical investigation was also made to analyze the influence of unconfined strength of concrete and tensile strength of CFRP wraps on the upgrade of compressive strength of composite column. It was observed that the use of high strength concrete and high tensile strength CFRP sheets has a positive effect on strength enhancement, however concrete with high strength can decrease the axial strain of the composite column. This paper has presented limitations for use of highly confined columns.

### *2.3.3. Tests of Concrete-Encased Steel Connections*

Karimi et al. (2012) investigated partially encased concrete-steel column encased in FRP jackets and the effect of slenderness parameter on the behavior of the composite column. In their paper, they observed that FRP confinement can increase the compressive strength of the concrete by 17%. They also proposed that confinement efficiency depends on the cross-sectional characteristics of the column. Their test results concluded that the compressive strength of the column was enhanced with the increase in column height; as they observed the failure of the longest column showed more ductility. The results obtained also show that the energy dissipation capacity of the composite column is greater than bare steel columns. The paper implied that the composite column can be used as a structural element to resist response under extreme dynamic loading.

## 2.4. Analytical Investigation (Finite Element Analysis)

It is interesting to simulate the behavior of the actual structure into an analytical model and obtain the behavior of the connections for better understanding. The analytical study reduces the time and investment in the experimental tests and numerous models with different parameter settings can be investigated in the analytical study. Some of the finite element analysis simulations in FRP retrofitting of beam, column, and connections will be discussed in this section.

### 2.4.1. *Study of Reinforced Concrete Beam and Column*

In order to study the performance of the concrete columns confined using FRP, much experimental and analytic work has been carried out. Hany et al. (2016) used the finite element (FE) software ABAQUS to simulate a FRP-confined concrete column. They suggested that the column can be modeled as a vertical slice with one end restrained against vertical translation instead of modeling the whole element. The interaction between FRP sheet which is designated as “LAMINA” material type and the concrete was modeled as a tie constraint so that nodes on both the surfaces are compelled to move similarly.

Ibrahim and Mahmood (2009) presented an FE model of RC beams externally reinforced with FRP laminates using ANSYS. They proposed three basic principles for using FRP materials for strengthening of concrete structures: (i) adding FRP to the tensile face to increase bending moment capacity; (ii) adding FRP laminates to shear tensile zones to increase shear capacity of beams; and (iii) encase columns with fiber composite materials around the perimeter to increase axial and shear capacity of the columns. For the finite element model, an ANSYS Solid65 element and smeared cracking approach was used to model the concrete. The reinforcing steel is designated as a Link8 element and bonding between concrete and steel was ensured by connecting nodes of each

adjacent elements so that both materials shares same nodes. FRP laminates have two constituents: reinforcement and matrix. To model FRP composites, an ANSYS Solid46 layered element was used. The connection between FRP and concrete shared same approach as of concrete and steel reinforcement. In another FE modeling approach done by Karim et al. (2009) using LS-DYNA, they used 8-node solid element for steel and concrete core whereas FRP jackets were modeled using four node shell elements.

#### 2.4.2. *Study of Riveted Connections*

Assessment of the strength and hysteretic capabilities of riveted and encased joints may show their significant contribution to seismic performance of old buildings (Naderi 2008). According to Naderi (2008), seismic behavior of old riveted connections is complex. Once the confined concrete loses its confining characteristics, the strength of the joint is taken by mere bare steel. The author concludes that understanding the possible failure modes in riveted connection is essential to predict the seismic behavior of the riveted joints. From his analytical analysis, he found out that, in T-stub joint as shown in Figure 12, there are many failure modes such as fracture of flange of T-section, fracture of tensile rivets, elongation of rivet holes, deformation of beam and column, etc. He assumed that the failure is influenced by uncertainty in tensile forces in rivets due to prying action. Under shear load, there is large deformation in rivet shank at shear plane. Whereas in clip angle joint system as shown in Figure 13, ultimate fracture involves fracture of rivets connecting top angle and column flange under tension loading and flexural yielding in the stem of the top angle, shear yielding of rivets and local buckling of column and beam flanges.

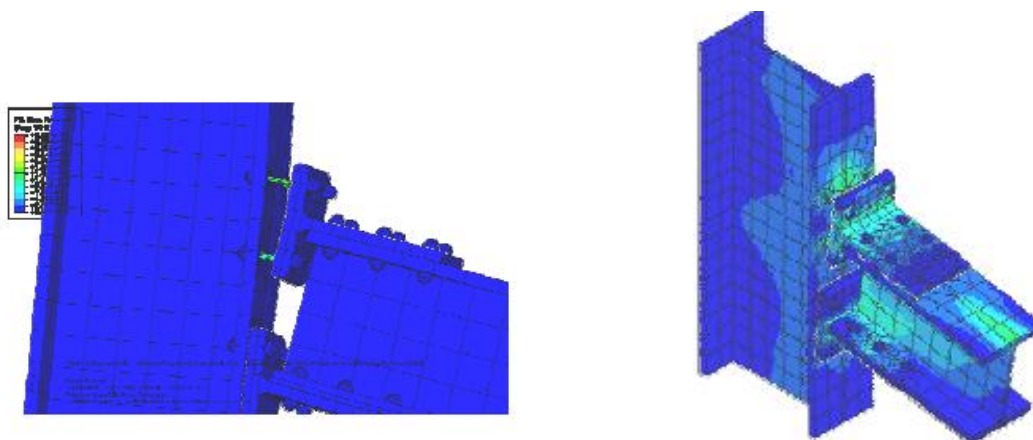


Figure 12. T-stub joint: rupture point under shear load (Naderi 2008)

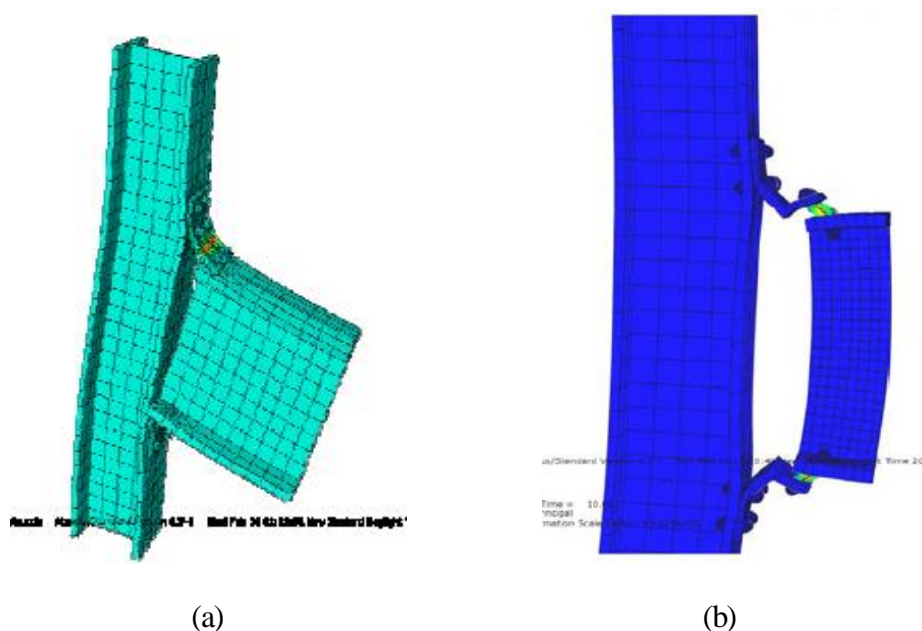


Figure 13. (a) Flexural yielding; (b) shear yielding; in clip angle joint under tension load (Naderi 2008)

Rodrigues et al. (2010) performed a FE analysis to access stresses in multiple rivet connections as shown in Figure 14. (a) FE model of multiple riveted connection; (b) Crack configuration (Rodrigues et al. 2010) using FE software ANSYS. The rivets and the plates were modeled as 20-noded hexahedral isoparametric element (SOLID95). The plate and rivet were connected using

surface to surface option (CONTACT174 and TARGET170). The frictional coefficient of 0.3 was adopted. The paper introduced the clamping stress effect of the rivet in the model by setting a preliminary load step with temperature variation ( $\Delta T$ ). This step defined orthotropic thermal expansion property of the rivet. The results obtained showed that the rivets close to the border are highest stressed.

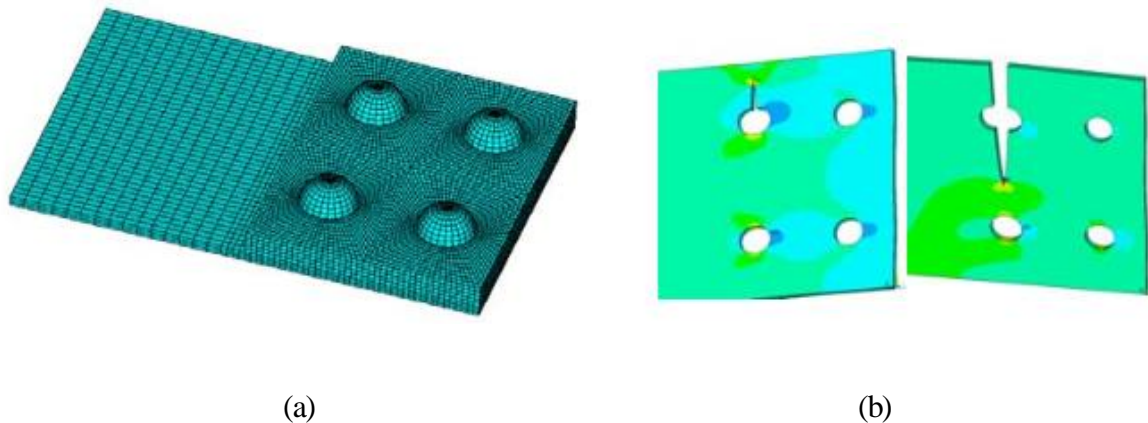


Figure 14. (a) FE model of multiple riveted connection; (b) Crack configuration (Rodrigues et al. 2010)

Imam et al. (2007) investigated the damage pattern in a riveted connection of a bridge using FE analysis with the commercial FE-code ABAQUS. They produced a 3-D FE model of a double lap, riveted joints with 8-noded brick elements. The contact between elements in an assembly was introduced using contact pair and master slave surface algorithm. The analysis considered a Coulomb friction model with frictional coefficient of 0.3. The rivet head was connected with plate in such a way that they were forced to remain in contact. A clamping stress was introduced in the rivet using “PRE-TENSION SURFACE” option in ABAQUS. This clamping stress is applied during the first step and external load act in addition to the pre-clamping stress in the second step.



The meshed double-lap riveted joint is shown in Figure 15 and the crack patterns observed after the analysis is given in Figure 16.

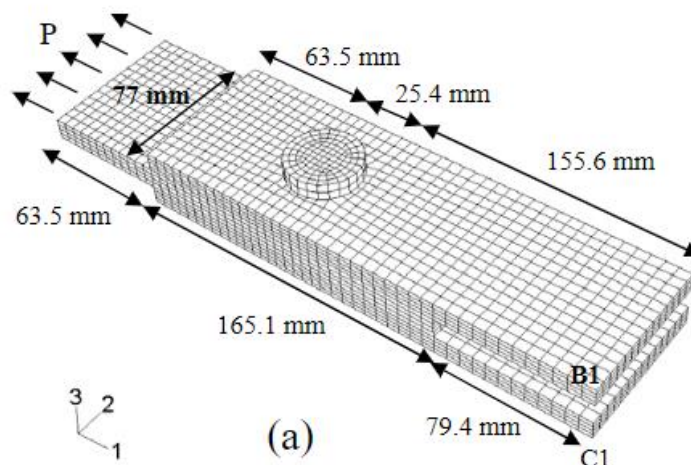


Figure 15. FE meshing of double-lap riveted joint (Imam et al. 2007)

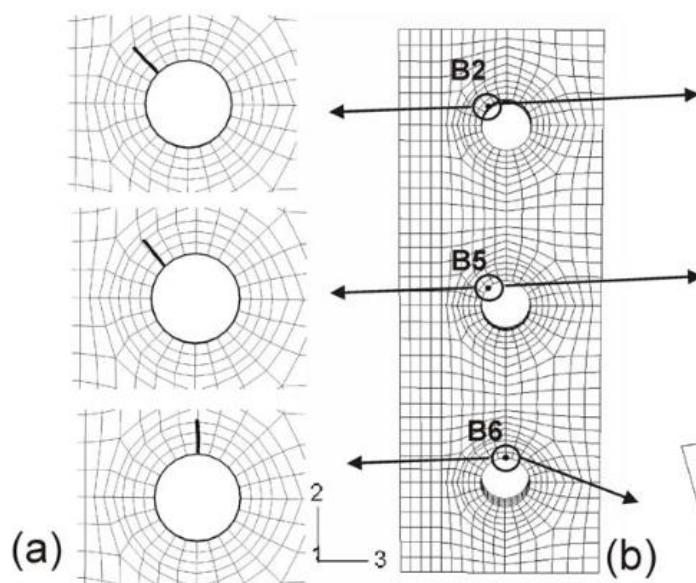


Figure 16. (a) Possible crack initiation pattern; (b) Fatigue crack initiation hot spots on holes  
(Imam et al. 2007)

In an experimental and numerical analysis study made by Pavan et al. (2011), riveted lap joints were analyzed for their static strength and load distribution in each rivet. The riveted joints were analyzed by non-linear finite element method to observe the geometric non-linearity effect in plate bending and yielding of plate and rivets. The lap joints with three, five, nine and twenty-five rivets were modeled using finite element software MSC/Nastran. The plates were modeled as plate elements and frictional effect between the two plates are neglected. The rivet holes were constrained using spring elements at the boundary to transfer load from plates to the rivets and vice-versa. The results showed that the riveted plate joints failed at the failure load where each rivet shared equal amount of load. They interpreted that rivets carry unequal load until they reach the elastic regime and once the rivet starts to yield, redistribution of load takes place resulting in nearly equal load in each rivet at the failure load. The failure of the riveted connection is shown in Figure 17 and the normalized load-deformation curve for different number of rivets is given in Figure 18.

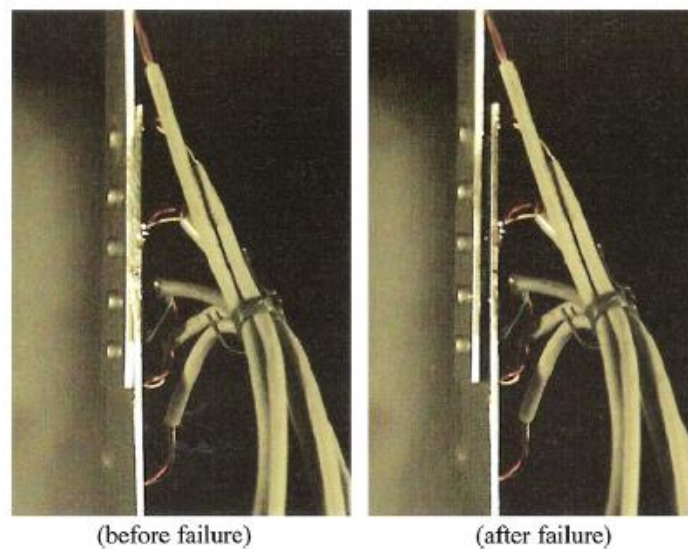


Figure 17. Lap joint with five rivets before and after failure (Pavan et al. 2011)

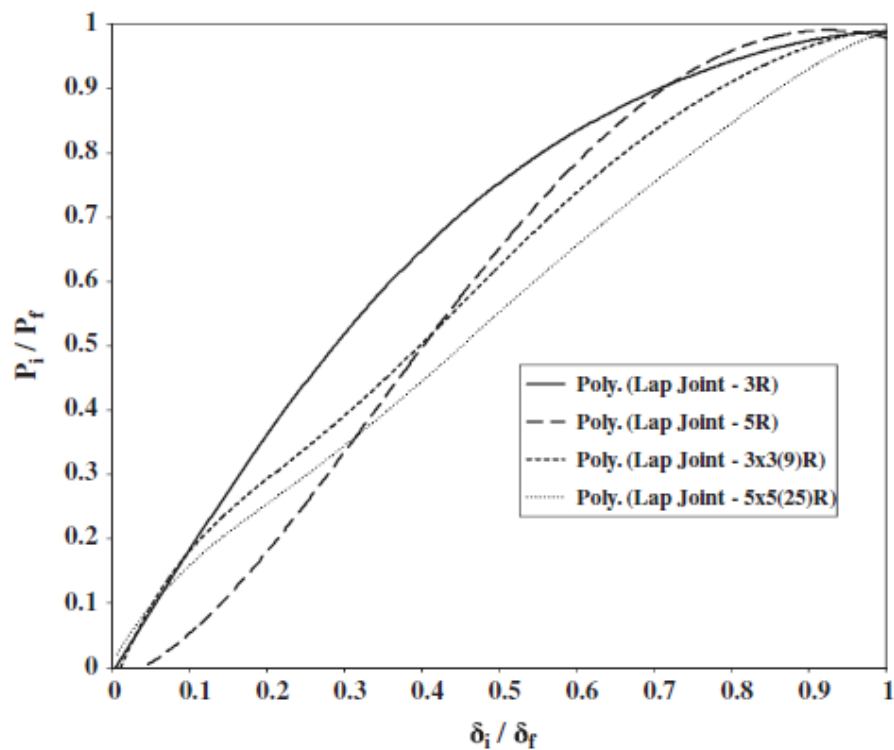


Figure 18. Normalized load-deformation curve for riveted joint, experimental (Pavan et al. 2011)

## CHAPTER III. FINITE ELEMENT ANALYSIS

### 3.1. Finite Element Analysis of Behavior of Riveted Lap Joint

The old steel frame connections of the Syndicate Building (see Chapter IV) consist of a Zee-shaped built-up column with riveted connections. It is necessary to understand the modeling requirements and behavior of riveted connections before analyzing the riveted beam-column connection for retrofitting strength. Thus, a finite element analysis of a lap joint model from Pavan et al. (2011) was done to compare against the experimental results.

#### 3.1.1. *Geometry and Material of Riveted Lap Joints*

As presented in Pavan et al. (2011), the Aluminum material was assigned to both the lap joint plates and the rivets with the properties as given in Table 1. The model consists of two aluminum plates connected with five rivets; each plate of 170mm x 40mm x 2mm in dimensions and rivets with 4 mm diameter in size. The plates consist of 5 rivet holes of 4 mm diameter and arranged at a distance of 15mm center to center as shown in Figure 19. The plates are modeled as a 3D solid element, SOLID186. SOLID186 element is a 20-node 3D solid element with three degree of freedom (translations in x, y and z directions) at each node. This element supports the plastic deformation and exhibit quadratic displacement behavior. The rivets were modeled as 3-D solid using SOLID187 element, which is a 10-noded element with three degree of freedom and is suited for modeling irregular meshes.

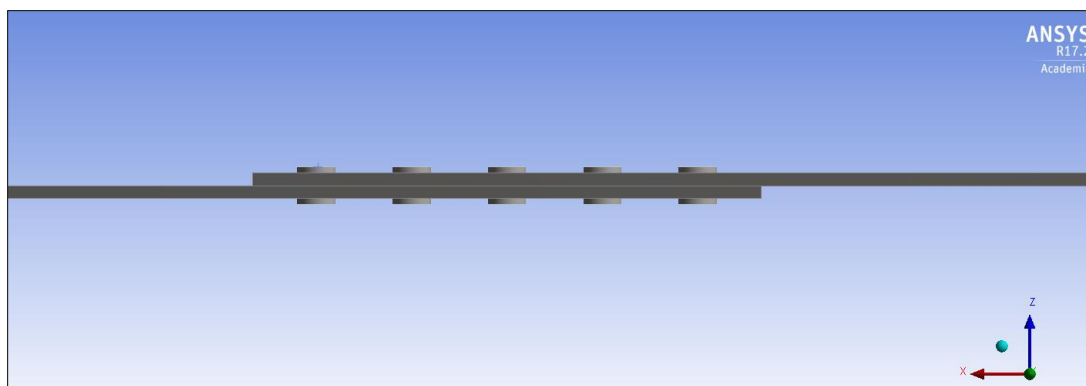


Figure 19. Geometry of single row five-rivet lap joint

Table 1. Material Properties of Elements Used in FE Analysis

Material	Modulus of Elasticity (GPa)	Poisson Ratio	Yield Strength (MPa)	Ultimate Tensile Strength (MPa)
Plate	72.34	0.33	324.8	441
Rivets	72.34	0.33	324.8	441

### 3.1.2. Finite Element Analysis of the Lap Joint

The riveted lap joint was modeled in the finite element software ANSYS Workbench V17.2 to study the behavior of the joint due to applied axial loading. 3D elements were used to model the plates and rivets using Design Modeler. The finite element analysis of the model was carried out to obtain the normalized load-deformation curve and compare with the experimental results from Figure 18. The contact between rivet shank and rivet hole was defined as a frictional contact with coefficient of friction taken as zero. The surface contact between two plates was defined as a frictionless contact. The plasticity of the joint plates was defined using bilinear isotropic hardening

property. In this analysis, the engineering stress-strain diagram as shown in Figure 20, which represents the stress-strain relationship of plate is used.

To ensure that the finite element results converges to an accurate solution and is independent of the mesh size, a convergence study was done. The model was meshed using coarser mesh and reducing the mesh size to smaller element size until the changing of mesh size does not affect the results of the analysis, which is called mesh convergence. Following convergence, the finite element model was meshed with 2 mm element size as shown in

Figure 21. The meshing resulted in total number of 8,222 elements and 43,449 nodes. One end of the plate was clamped against translation and rotation in all three directions and the other end of the plate was pulled by an axial force  $P$ . The load was gradually applied with load increasing with each sub-step.

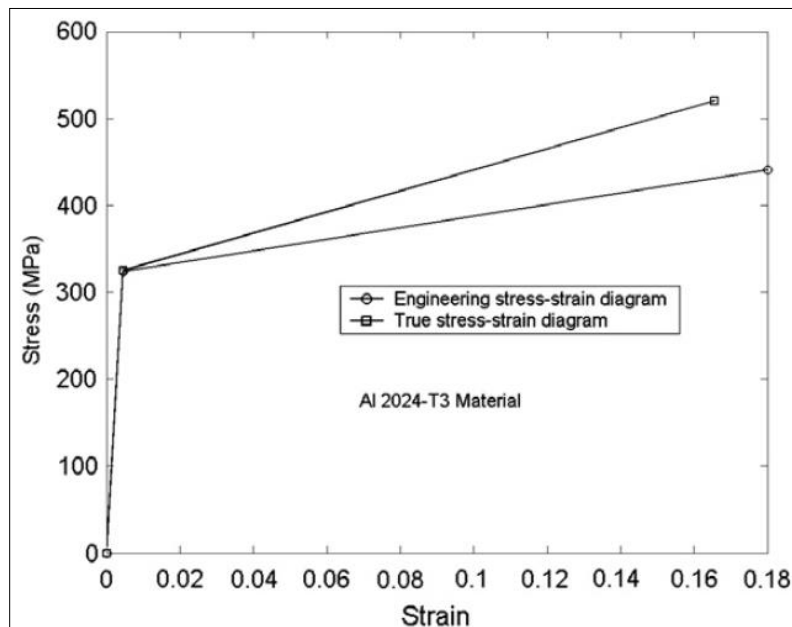


Figure 20. Stress-strain relationship used for plates (Pavan et al., 2011)

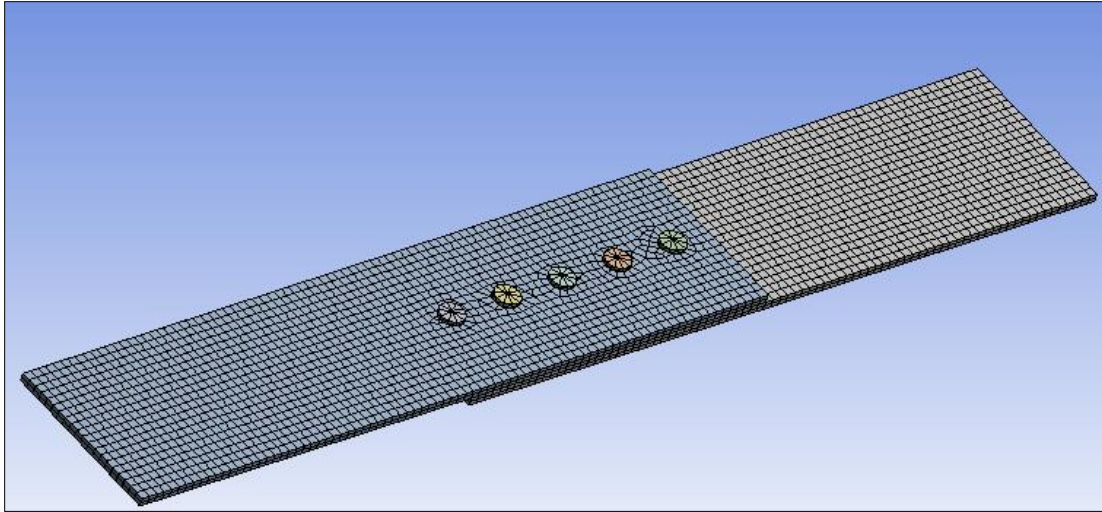


Figure 21. ANSYS finite element mesh for riveted lap joint

### 3.1.3. Analysis Results

The finite element analysis of the lap joint model predicted the failure of the model at axial load of value 19.1kN. The failure load obtained by Pavan et al. (2011) in their experiment was 17.93kN which is smaller than the value obtained in the analysis, but the behavior of riveted joint in the analysis is very close to the experimental results. The normalized load-deformation curve obtained from the FEA and experimental results of Pavan et al. 2011 is plotted in Figure 22 and is compared against each other. The x-axis of the curve represents the normalized load displacement ( $d_i/d_f$ ) which is the displacement ( $d_i$ ) obtained at each load increment normalized with the joint displacement ( $d_f$ ) at the failure load. Similarly, y-axis represent the normalized load ( $P_i/P_f$ ) i.e. applied incremental load ( $P_i$ ) normalized with the failure load ( $P_f$ ) of the corresponding lap joint. The similarity in the pattern of both the curves observed in the graph corroborate the validation of the model. The reason behind the observation of higher failure load is likely related to the material properties that was used in the analysis. Pavan et al. (2011) stated the use of Al 2024-T3 material

for the plates and rivets, however the Modulus of Elasticity and basic material property was not given in the paper. Thus, the default Aluminum alloy material available in the ANSYS file was assigned to the plate element in finite element analysis, which could have altered the results somehow.

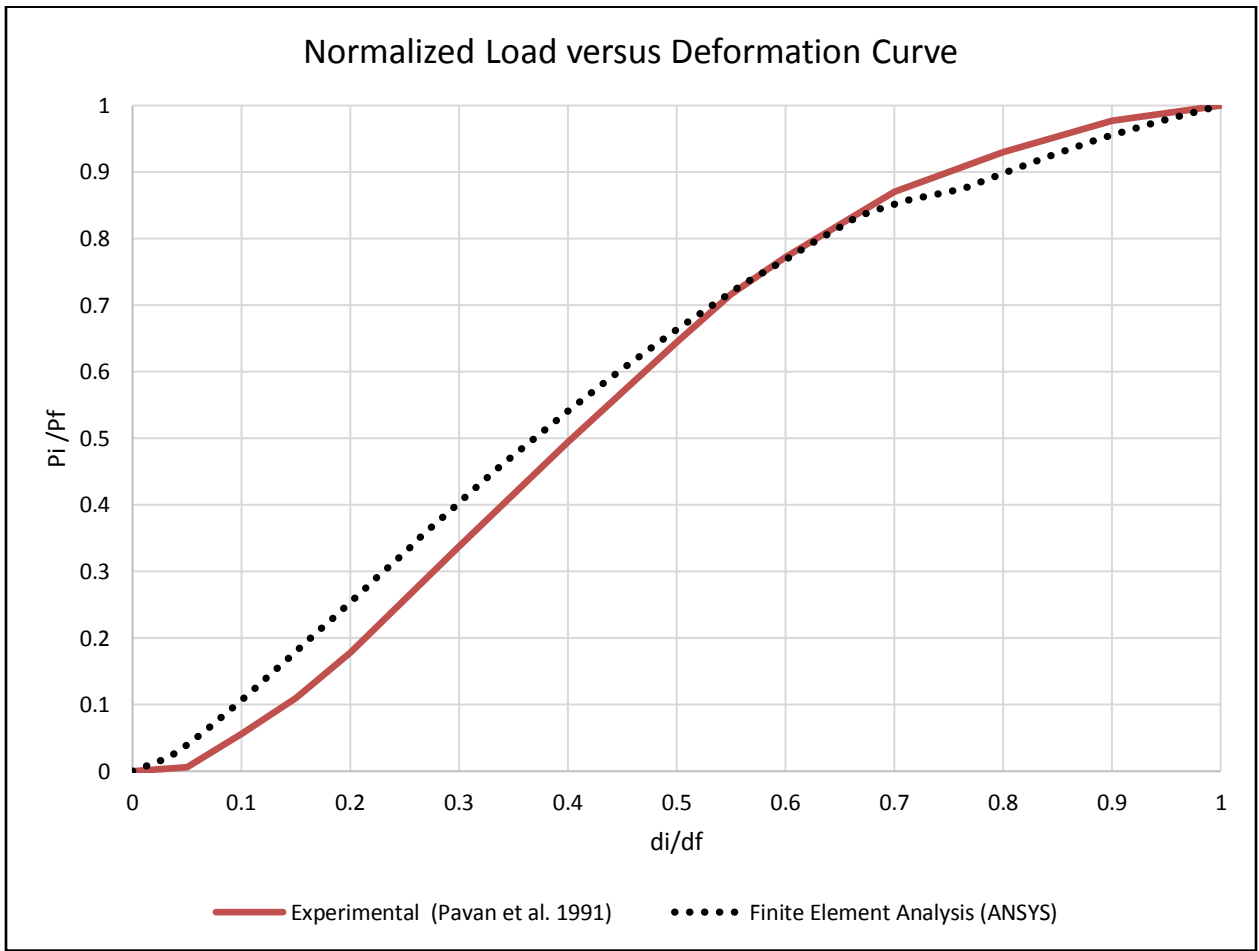


Figure 22. Normalized load versus deformation (Experimental by Pavan et. al and ANSYS)

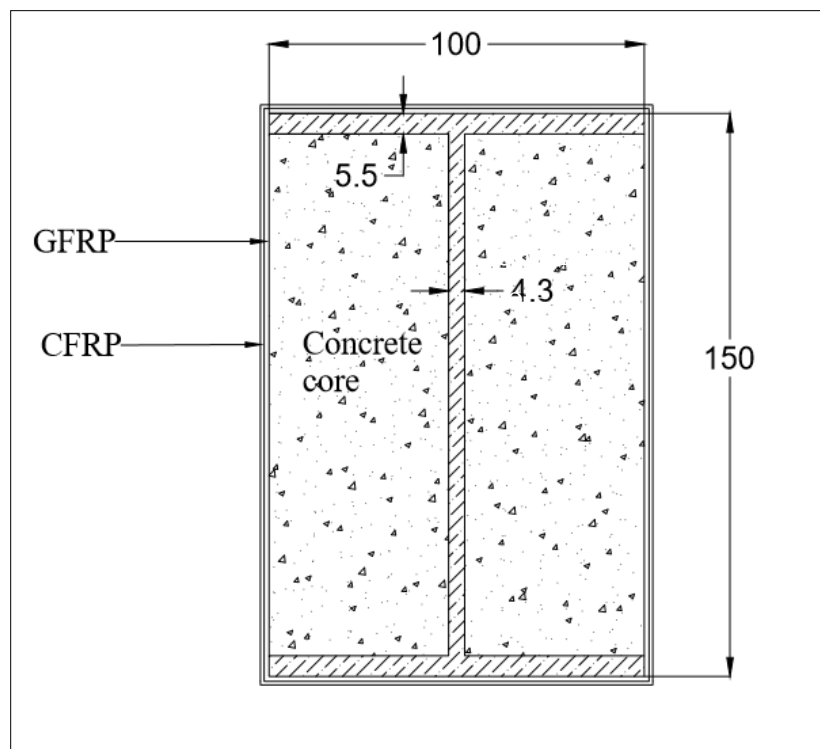


### 3.2. Finite Element Analysis of Steel Column with Concrete-Filled Composite Jackets

There has not been much research on the retrofitting of concrete-encased steel columns with the application of FRPs. However, in some of the research papers, steel columns were enveloped in FRP sheets to prevent the buckling of the column. Karimi et al. (2011) have done an experimental and analytical study on wrapping the steel column with one layer of GFRP and an additional layer of CFRP for the retrofitting purpose. Later the resulting void was filled with concrete. The model analyzed in this paper was similar to concrete-encased steel column with an I-section steel column with concrete encasement. Due to the similarity in both the models, it was found essential to initially replicate the finite element analysis on the model presented in their paper to validate the idealization of the model for the final project model.

#### 3.2.1. *Geometry and Material Properties*

The steel column used in the analysis was a 500 mm long W150x14, wrapped with one layer of GFRP and an additional layer of CFRP as shown in Figure 23. The steel column was assigned with Structural Steel material with yield strength of 411 MPa and ultimate tensile strength of 526 MPa. The 28-day compressive strength of concrete was taken as 44 MPa. The non-linear behavior of the steel was defined by “Linear Isotropic” and “Bilinear Isotropic”. The linear isotropic properties include Young’s Modulus of elasticity and Poisson’s ratio whereas bilinear isotropic properties include yield stress and tangent modulus, which is given in Figure 24.



(All dimensions are in mm)

Figure 23. Geometry of composite column

Properties of Outline Row 9: Structural Steel			
	A	B	C
1	Property	Value	Unit
2	Density	7850	kg m <sup>-3</sup>
3	Isotropic Secant Coefficient of Thermal Expansion		
4	Coefficient of Thermal Expansion	1.2E-05	C <sup>-1</sup>
5	Zero-Thermal-Strain Reference Temperature	22	C
6	Isotropic Elasticity		
7	Derive from	Young's Modulus...	
8	Young's Modulus	2E+05	MPa
9	Poisson's Ratio	0.3	
10	Bulk Modulus	1.6667E+11	Pa
11	Shear Modulus	7.6923E+10	Pa
12	Bilinear Isotropic Hardening		
13	Yield Strength	400	MPa
14	Tangent Modulus	0	MPa

Figure 24. Material properties for steel model

The linear property of the concrete is provided in Figure 25. “Multilinear Isotropic Hardening” property is assigned that defines the stress-strain behavior of the concrete up to crushing. Figure 26 shows the multilinear isotropic stress-strain diagram of unconfined concrete used in the model analysis using the equation expressed by MacGregor (1992). The FRP sheets were assumed to be unidirectional fabrics having material properties mentioned in Table 2.

The FRPs were assumed to show linear elastic behavior till rupture. The value for Young’s modulus in the hoop direction was defined with the value given by the manufacturer whereas the value of modulus of elasticity and shear modulus in other direction were assigned small values as shown in Figure 27. The I-section column and concrete cylinder were modeled as a 3D SOLID185, an eight-node homogenous element having three degree of freedom at each node. The FRP laminates were treated as a thin shell element SOLSH 190. This element is an eight-node element with three degree of freedom at each node.





Properties of Outline Row 5: Concrete			
	A	B	C
1	Property	Value	Unit
2	 Material Field Variables	 Table	
3	 Density	2300	kg m <sup>-3</sup> ▼
4	 Isotropic Elasticity		
5	Derive from	Young's Modulus... ▼	
6	Young's Modulus	28000	MPa ▼
7	Poisson's Ratio	0.19	
8	Bulk Modulus	1.5054E+10	Pa
9	Shear Modulus	1.1765E+10	Pa

Figure 25. Linear material properties for concrete model

Table 2. Material Properties of FRP

	Tensile Strength (MPa)	Modulus of Elasticity (GPa)	Thickness (mm)
GFRP Sheet	575	26.1	1.3
CFRP Sheet	876	72.4	1.0

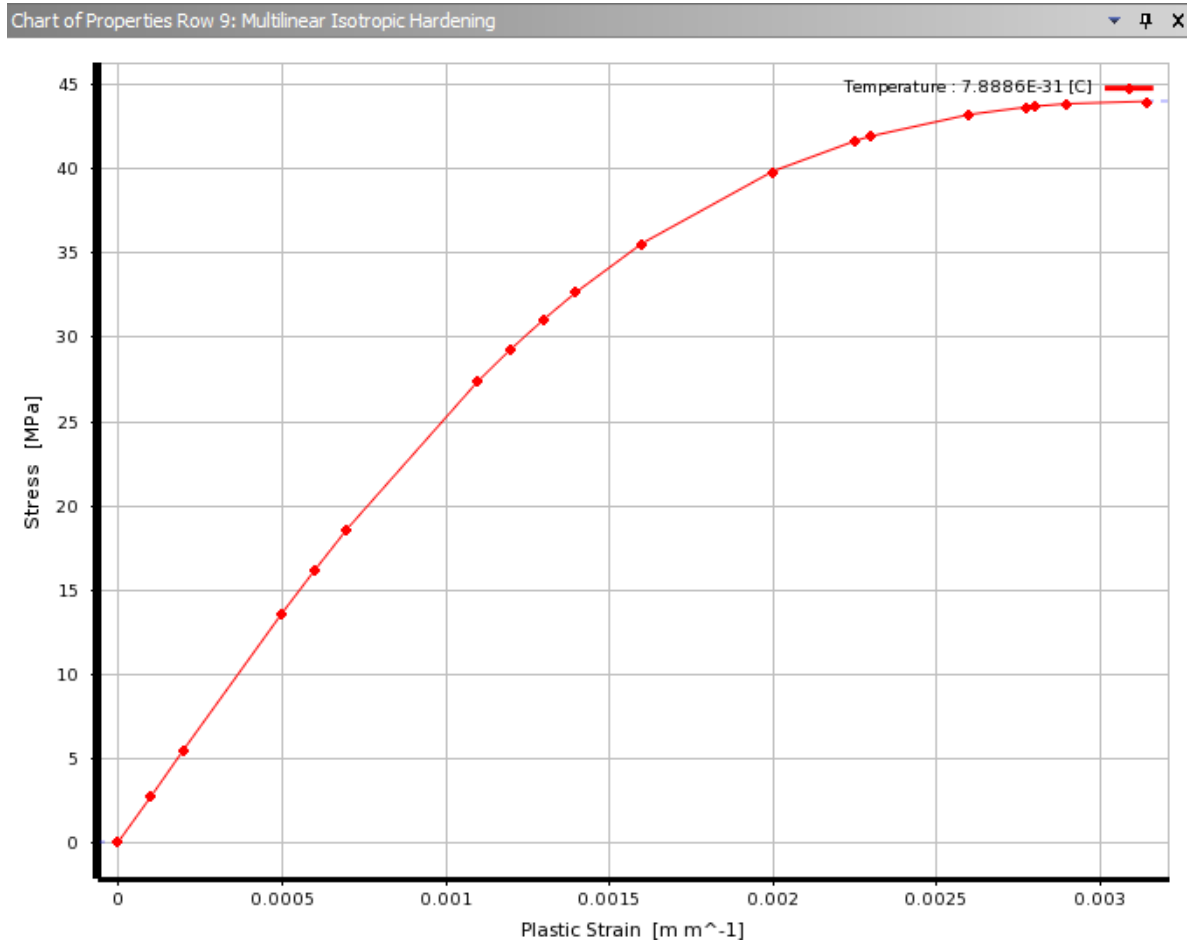


Figure 26. Stress-strain graph of concrete used in ANSYS according to MacGregor (1992).



Properties of Outline Row 4: CFRP-Y			
	A	B	C
1	Property	Value	Unit
3	 Density	1521.8	kg m <sup>-3</sup> ▼
4	 Orthotropic Elasticity		
5	Young's Modulus X direction	1000	MPa ▼
6	Young's Modulus Y direction	72400	MPa ▼
7	Young's Modulus Z direction	1000	MPa ▼
8	Poisson's Ratio XY	0.1	
9	Poisson's Ratio YZ	0.1	
10	Poisson's Ratio XZ	0.2	
11	Shear Modulus XY	3000	MPa ▼
12	Shear Modulus YZ	3000	MPa ▼
13	Shear Modulus XZ	3000	MPa ▼

Figure 27. Orthotropic elasticity property of CFRP in Y-direction

### 3.2.2. Finite Element Analysis of Composite Column

The composite column was modeled in ANSYS V17.2 to obtain the axial load-displacement behavior of the column. The wrapping of FRP laminates around the concrete provided a level of confinement around the concrete which increased the strength of confined concrete. The FRP sheets were perfectly elastic (see Table 2 for elastic properties). The connection between GFRP and steel column, and CFRP and GFRP was selected as “BONDED” contact which is a contact element acting like a glue that holds the bodies together. No contact definition was assigned to the contact surface of concrete to the steel.

Following the mesh convergence, the composite column was uniformly meshed with an element size of 20mm, 10mm and 7 mm, respectively until the results from the analysis was almost similar for 10mm and 7 mm. The final meshed model with an element size of 7 mm is shown in Figure 28. The meshing resulted into total number of 34416 elements and 54750 nodes. The bottom of the column was restrained against translational and rotation within all three-axis using fixed boundary

condition. An incremental displacement was applied at the top reference point of the composite column in longitudinal direction to investigate the axial deformation of the column.

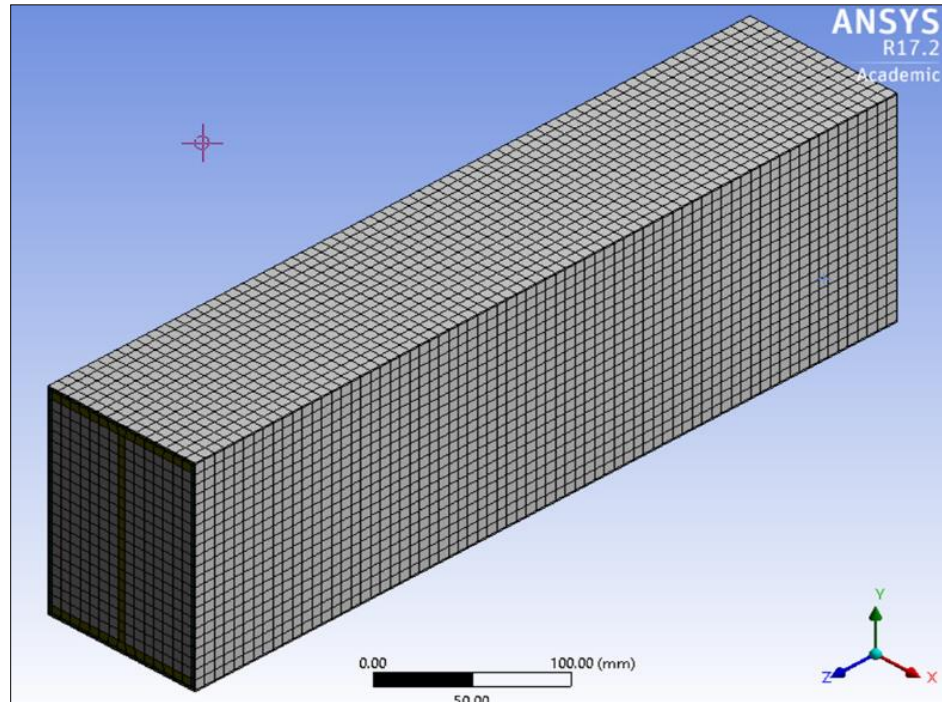


Figure 28. Finite Element Meshing of the Composite Column

### 3.2.3. Analysis Results

The axial load-displacement curve obtained from FEA of the composite column is plotted against the experimental and analytical results from Karimi et al. (2011) in Figure 31. The graph showing the axial load-displacement diagram of the control specimens of steel column without any concrete (C1-0, C2-0) is adopted in this paper from Karimi et al. (2011) as shown in Figure 29. The letter “C” denotes the control specimen and the following digit in the code indicate the specimen number.

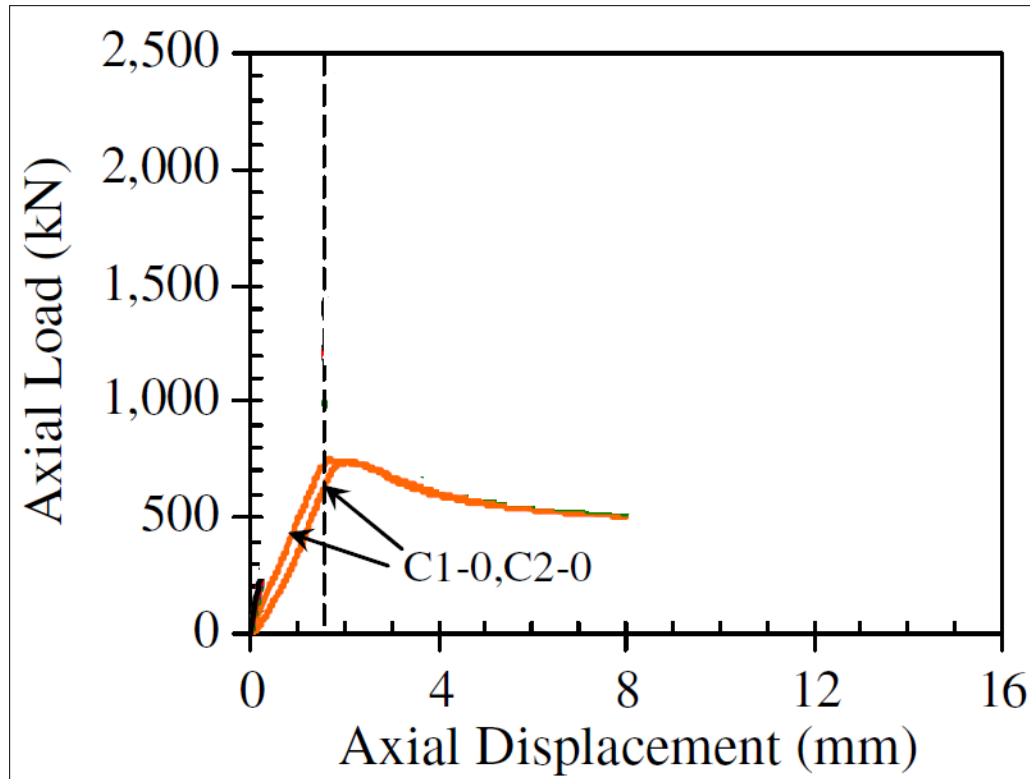


Figure 29. Axial Load-displacement curve of the control specimen (Karimi et al. 2011)

In the analytical study, Karimi et al. (2011) prepared an analytical model of the composite column to study the axial load-deformation behavior of the model. The analytical model assumed the steel property to be elastic-perfectly plastic, which is represented in Figure 30(a). The wrapping of FRP sheets around the concrete provided a confinement of concrete that results to an increased concrete strength. The confined compressive strength of the concrete was assumed to be linearly proportional to the confining pressure. The stress-strain relationship of confined concrete used in the analytical study is the relationship expressed by Lam and Teng (2003a) and is given in Figure 30(b). The failure of the composite column was characterized by the FRP rupture that led to concrete crushing. The ultimate strain of the composite column was calculated using an expression that relates it with the confinement pressure and confinement stiffness ratio. The ultimate strength-

strain values obtained in the study was employed to develop the corresponding axial load-deformation graph for the column, which is shown in Figure 31.

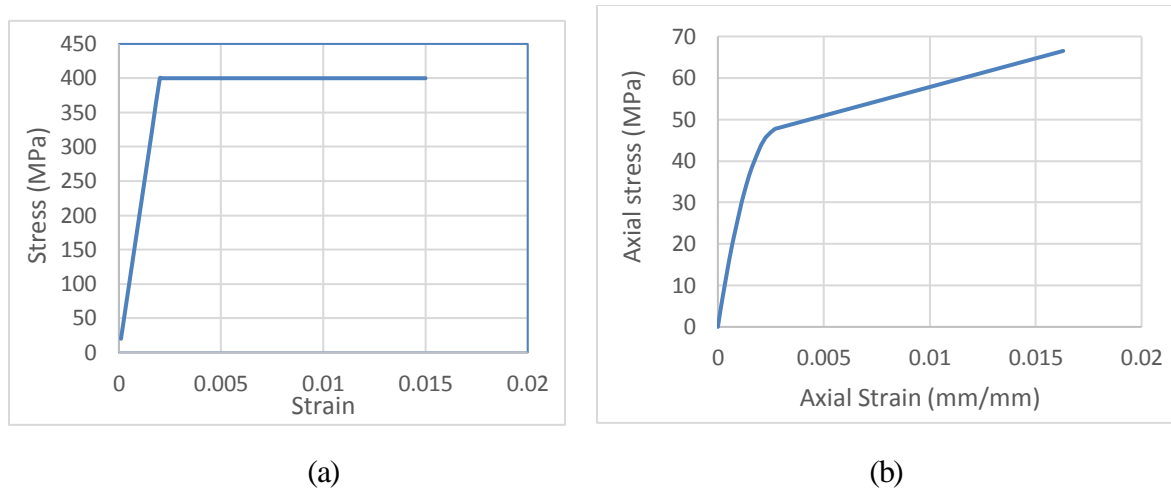


Figure 30. Stress-strain relationship for (a) steel; (b) confined concrete; used in the analytical study (Karimi et al. 2011)

Comparing the load-deformation graphs of the control specimen of column and the one obtained from finite element analysis of the composite column, the obtained ultimate strength of bare steel column was 700kN load whereas for the composite column was 1537kN load. The results showed that the ultimate strength of the composite column was almost two times of the strength of the steel column. The increased compressive strength of the confined concrete due to FRP confinement is primarily responsible for the increased strength of the composite column. Figure 31 shows the results obtained from the finite element analysis performed in ANSYS and analytical results from Karimi et al. in comparison with the experimental results. It was seen that the nature of the graph obtained in the FEA was in good agreement with the experimental and analytical results. This supports the validation of the FEA model of the composite column.



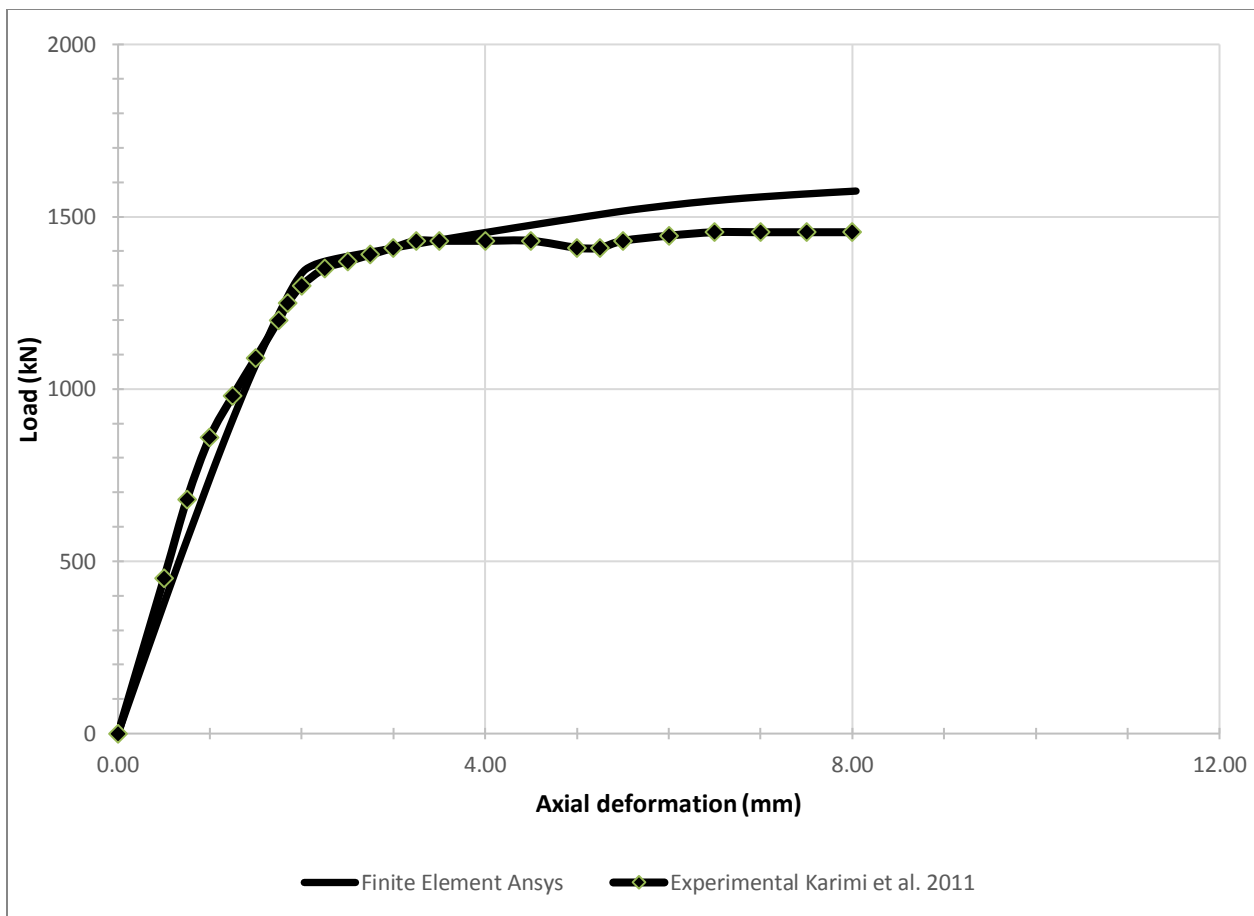


Figure 31. Axial Load-Displacement Curve obtained from ANSYS FEA vs. Experiment

## CHAPTER IV. ANALYSIS OF CONCRETE-ENCASED BEAM-COLUMN CONNECTION

### 4.1. Introduction to the Syndicate Building

The Syndicate Trust Building, commonly called as *The Syndicate* is an old historic building built in 1906 and is situated in the downtown St. Louis, Missouri. The Syndicate was added to the National Register of Historic places in 2002. The Syndicate once became vacant in 1967 and was reconstructed between 2006 and 2008 to hold luxury condos in a project. The building now consists of 94 condominiums, 84 apartments, street level retail and parking in the basement and first two floors of the buildings (Wikipedia, 2019).

The building is a sixteen-story building with an attic and a basement as shown in Figure 32 . The building uses blond brick and terra cotta for the exteriors. The south and north elevations are ten bays wide and the west elevation is 18 bays. The floor elevation, floor plan and the typical beam-column section, obtained from the construction drawing of the Syndicate Building are given in Figure 33, Figure 34 and Figure 35, respectively.

### 4.2. General Description of Beam-Column Joint of the Syndicate Building

The beam-column connection used for the analysis was obtained from the Syndicate building. The moment frame of the Syndicate building consists of a concrete-encased steel beam-column joint, the typical cross-sections of which is given in Figure 35. The cross-section of the exact beam-column connection considered in the analysis is shown in Figure 36.



Figure 32. The Syndicate Trust Building (Original building drawing provided by KPFF)

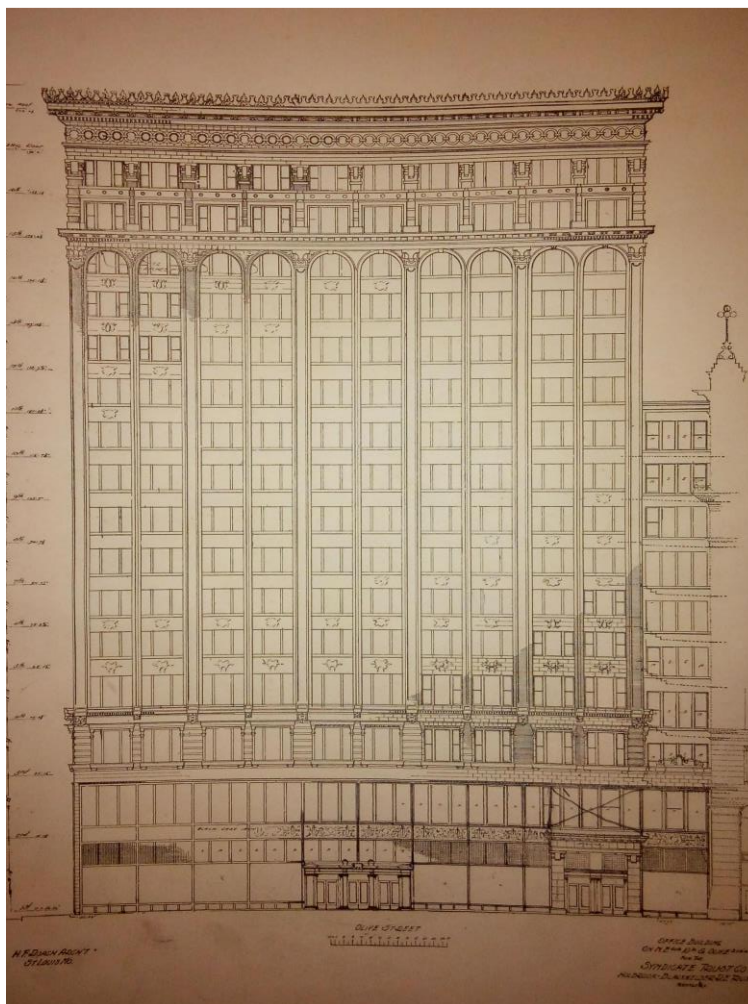


Figure 33. Floor elevation of the building (Original building drawing provided by KPFF)

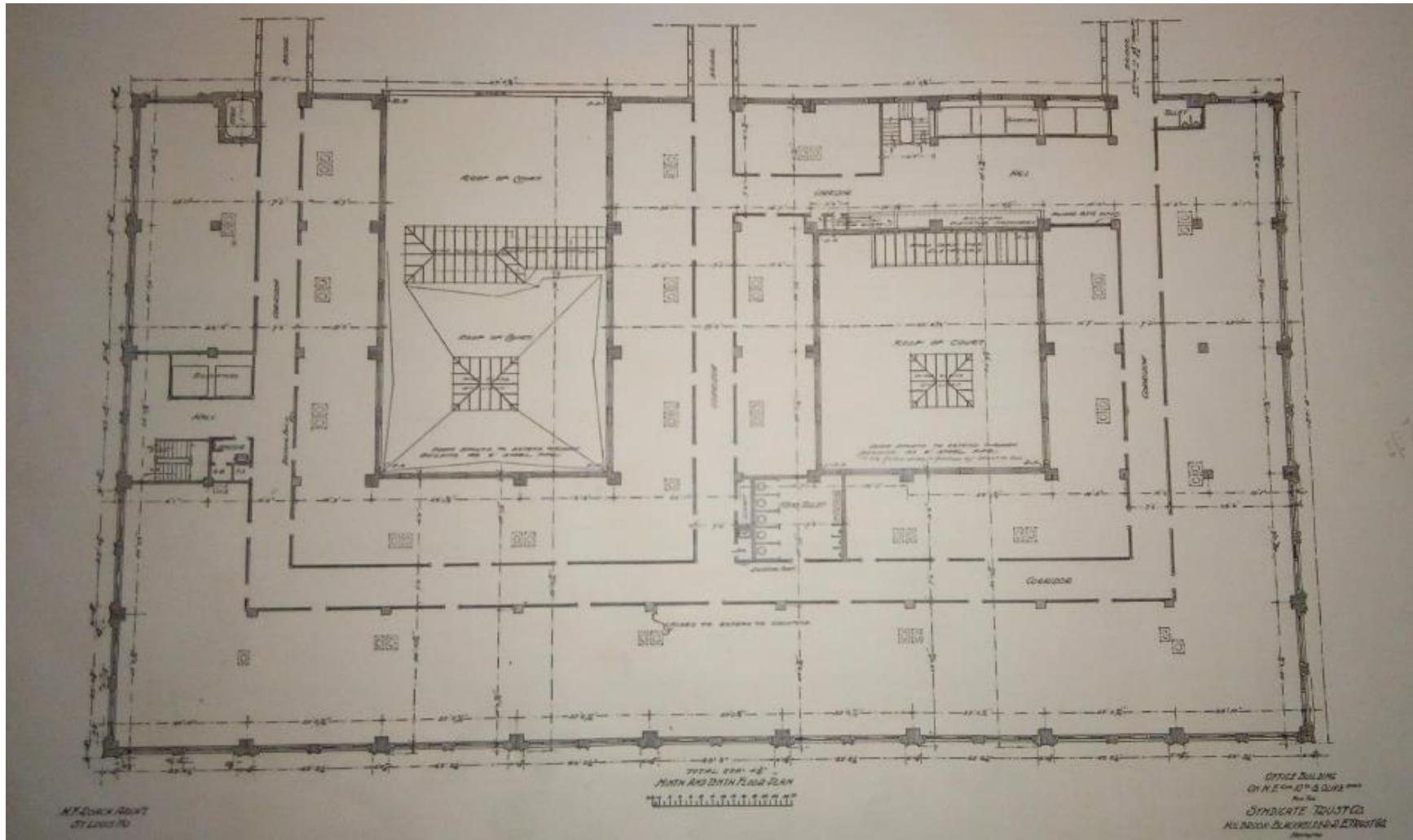


Figure 34. Ground floor plan of the building (Original building drawing provided by KPFF)

The column of the joint is a built-up column made up of Z-sections and steel plate connected via steel rivets as shown in Figure 37. From the figure, four 4-inch Z-sections are connected with a 7½” width steel plate of ¼” thickness using rivets of ¾” diameter to form a built-up column. The steel beam size used in the connection is a W8x35, which is connected to the column with an L-shaped connector using rivets. The cross-section detail of I-section, Z-section and L-section is provided in Figure 38. The steel frame is encased inside low strength concrete to provide confinement. The beam of the connection was found to be a T-shaped beam with a 4-inch thick slab, which has been incorporated in the model for the analysis. The cross section of the connection including slab has been shown in Figure 39.

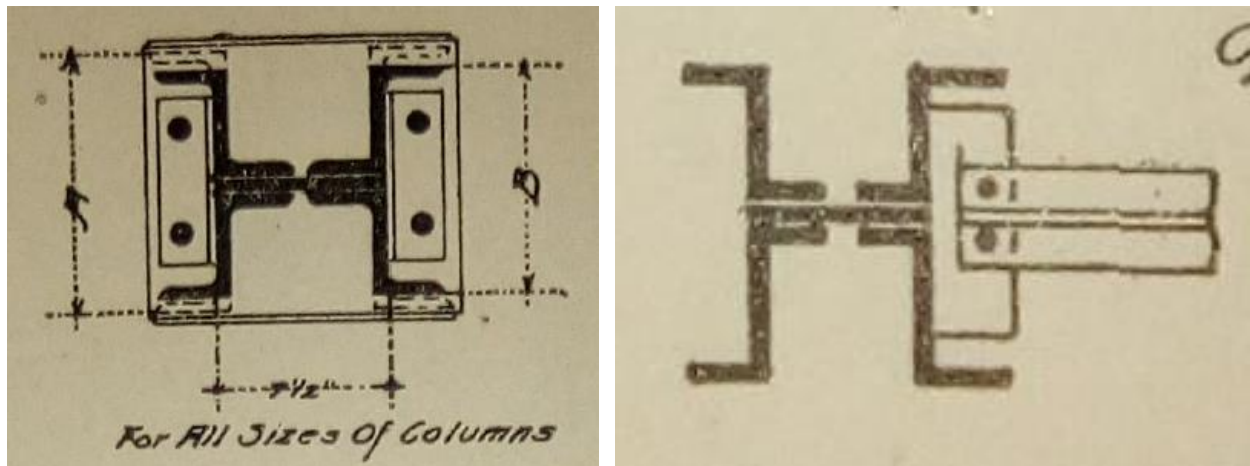


Figure 35. Typical beam-column section (Original building drawing provided by KPFF)

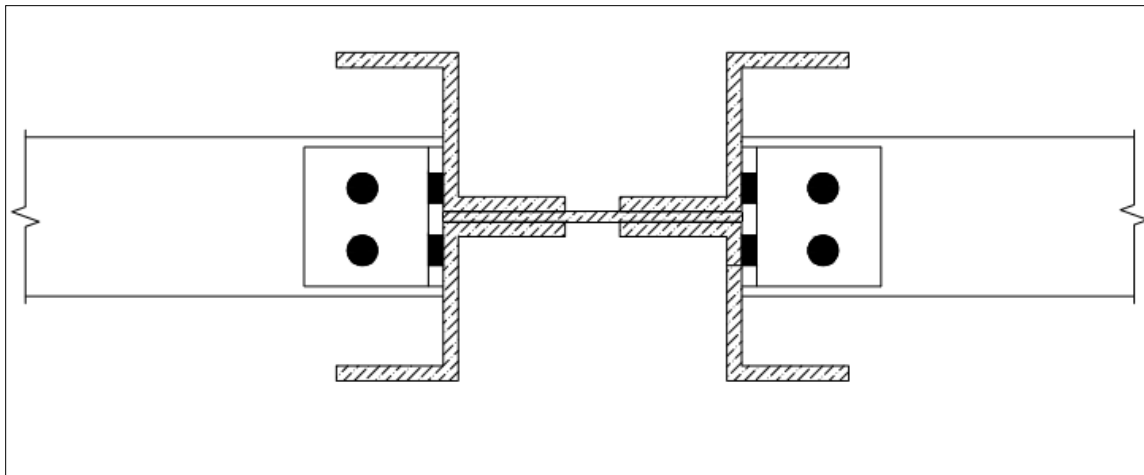
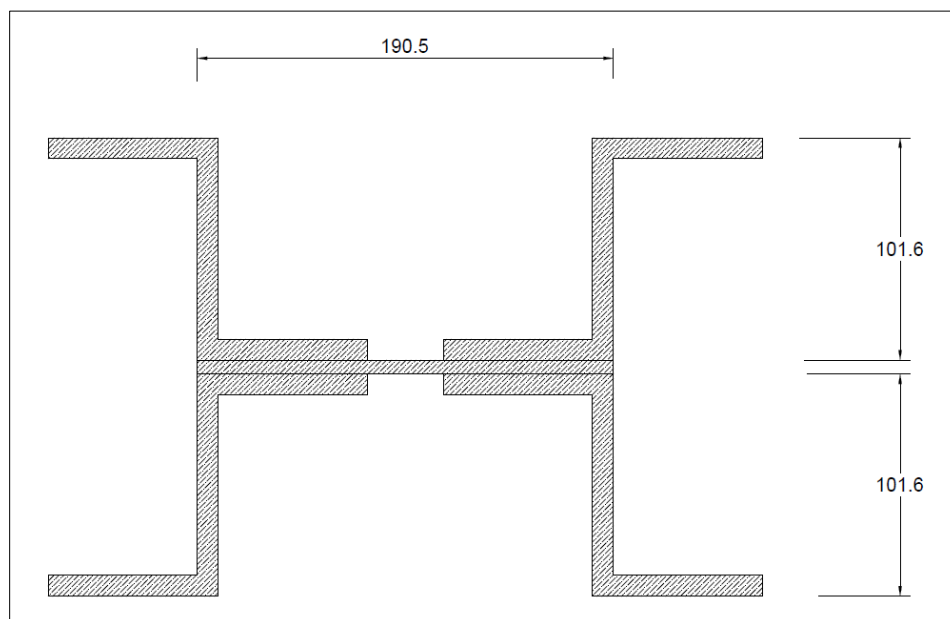
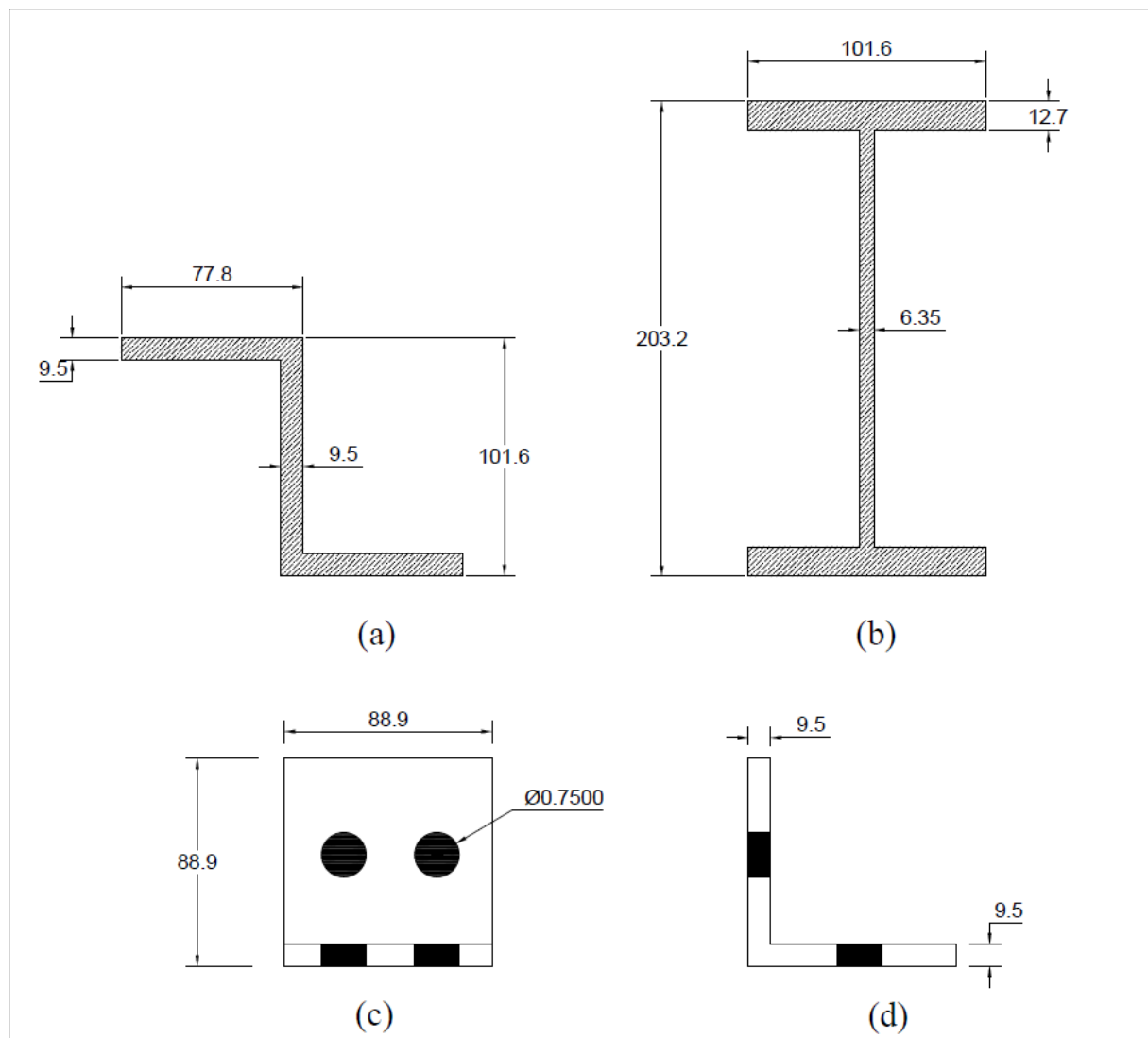


Figure 36. Cross-section detail of steel beam-column connection



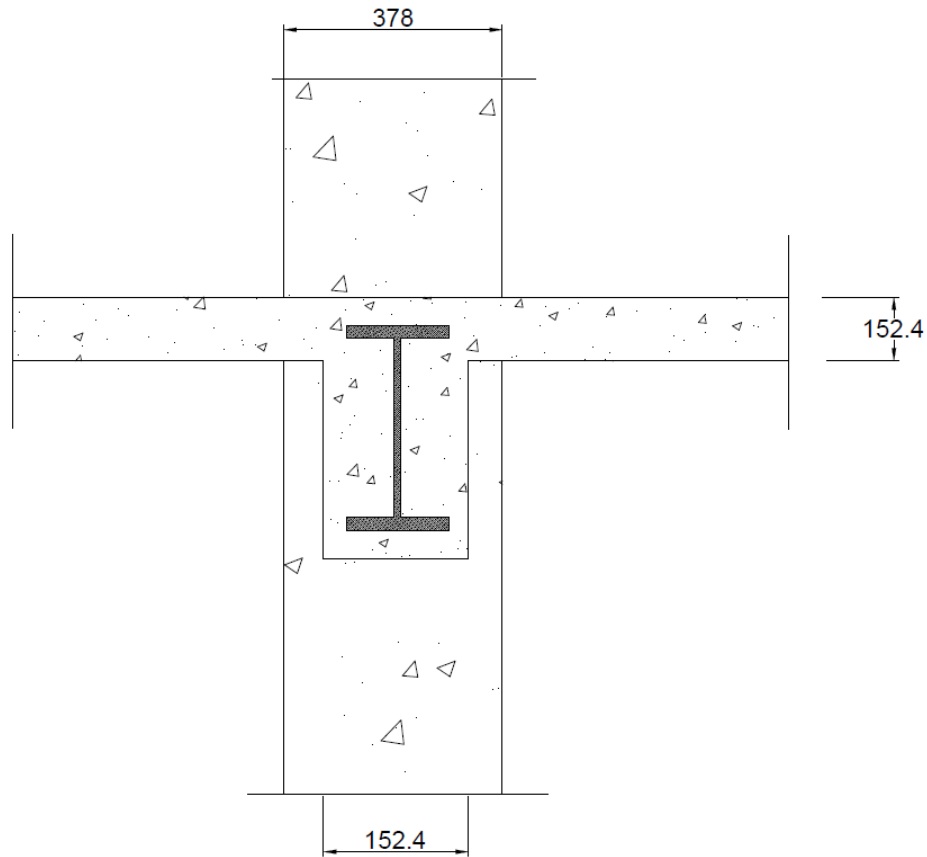
(All dimensions in millimeters)

Figure 37. Cross-section of built-up column



(All dimensions in millimeters)  
 (Diameter of hole in inch)

Figure 38. Typical cross-section of (a) Z-section; (b) I-section; (c) Plan of L-section;  
 (d) Cross-section of L-section



(All dimensions in millimeters)

Figure 39. Typical section of concrete-encased connection

#### 4.3. Finite Element Analysis of Beam-Column Connection

This section will introduce the finite element analysis of the concrete-encased beam-column connection to study load, displacement and moment carrying capacity of the connection before and after the application of the FRP. A total of five models were analyzed using finite element analysis software ANSYS; two concrete-encased models were used as control specimens and three concrete-encased joints were retrofitted using FRP system. The description of all the models will be discussed here in this section. It will summarize the set of finite element parameters used in knowledge to conduct the analysis, key requirements for proper idealization of the model and



discusses the analysis results. The finite element analysis was performed on the concrete-encased steel section (with and without FRP wrapping). Details regarding the adopted material properties, geometry and finite element idealization of each analysis will be provided in the next section.

#### 4.4. Finite Element Analysis of Concrete-Encased Beam Column Connection

##### 4.4.1. *Description of Finite Element Model of Bare Steel Connection*

The steel column was a 1500 mm long built-up column connected on each side to a 1200mm long W8x35 beam with L-shaped connector as shown in Figure 36. The properties of the steel and rivets need to be accurate in order to predict the actual behavior of the moment connection. The material properties of the structural steel (early 1900s) was thus adopted from ASCE 41-17. The steel used in the analysis is a perfectly elastic-plastic material with the yield strength of each material as mentioned in Table 3.

Table 3. Material Properties of Steel (ASCE 41-17)

<b>Material</b>	<b>Modulus of Elasticity (GPa)</b>	<b>Yield Strength (MPa)</b>
<b>Rivet Steel</b>	200	206.84
<b>Structural Steel</b>	200	193.05
<b>Plates</b>	200	227.53

The non-linear behavior of the structural steel, steel plate and rivet steel were defined using “Linear Isotropic” and “Bilinear Isotropic” property. The linear isotropic properties include Young’s Modulus of elasticity and Poisson’s ratio whereas bilinear isotropic properties include yield stress and tangent modulus, which is given in Figure 40, Figure 41 and Figure 42, respectively, for rivet, steel plate and structural steel. The I-section beam, L-shaped connectors, Z-shaped column and the

steel plate were modelled as SOLID 185 element. SOLID 185 is an eight-node homogenous element having three degree of freedom at each node. The rivets of the connection were assigned SOLID285 element, which is a lower order 3D, 4-node element suitable for modeling irregular meshes usually generated by various CAD systems.

Properties of Outline Row 5: rivet steel			
	A	B	C
1	Property	Value	Unit
2	Density	54.463	kg m <sup>-3</sup>
3	Isotropic Secant Coefficient of Thermal Expansion		
4	Coefficient of Thermal Expansion	1.2E-05	C <sup>-1</sup>
5	Zero-Thermal-Strain Reference Temperature	22	C
6	Isotropic Elasticity		
7	Derive from	Young's Modulus and Poisso...	
8	Young's Modulus	1.9995E+05	MPa
9	Poisson's Ratio	0.3	
10	Bulk Modulus	1.6662E+11	Pa
11	Shear Modulus	7.6903E+10	Pa
12	Bilinear Isotropic Hardening		
13	Yield Strength	206.84	MPa
14	Tangent Modulus	0	MPa

Figure 40. Material properties for rivet model

Properties of Outline Row 6: Steel plate			
	A	B	C
1	Property	Value	Unit
2	Density	54.463	kg m <sup>-3</sup>
3	Isotropic Secant Coefficient of Thermal Expansion		
4	Coefficient of Thermal Expansion	1.2E-05	C <sup>-1</sup>
5	Zero-Thermal-Strain Reference Temperature	22	C
6	Isotropic Elasticity		
7	Derive from	Young's Modulus and Poisso...	
8	Young's Modulus	1.9995E+05	MPa
9	Poisson's Ratio	0.3	
10	Bulk Modulus	1.6662E+11	Pa
11	Shear Modulus	7.6903E+10	Pa
12	Bilinear Isotropic Hardening		
13	Yield Strength	227.53	MPa
14	Tangent Modulus	0	MPa

Figure 41. Material properties for steel plate model

Properties of Outline Row 8: Structural Steel 2			
	A	B	C
1	Property	Value	Unit
2	Density	54.463	kg m <sup>-3</sup>
3	Isotropic Secant Coefficient of Thermal Expansion		
4	Coefficient of Thermal Expansion	1.2E-05	C <sup>-1</sup>
5	Zero-Thermal-Strain Reference Temperature	22	C
6	Isotropic Elasticity		
7	Derive from	Young's Modulus and Poisso...	
8	Young's Modulus	1.9995E+05	MPa
9	Poisson's Ratio	0.3	
10	Bulk Modulus	1.6662E+11	Pa
11	Shear Modulus	7.6903E+10	Pa
12	Bilinear Isotropic Hardening		
13	Yield Strength	193.05	MPa
14	Tangent Modulus	0	MPa

Figure 42. Material property for structural steel model

The geometry of the entire connection from ANSYS file is shown in Figure 44 and the closer view of the connection is given in Figure 43. The rivets were connected with the rivet hole using surface to surface option (CONTACT174 and TARGET170). All the other steel sections surface was assumed to be have no contact forces between them.

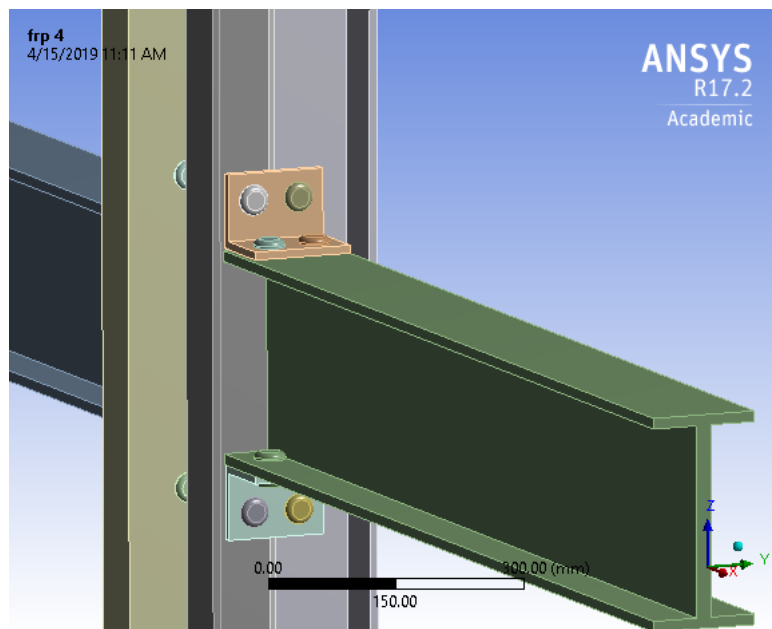


Figure 43. Closer view of riveted connection of the joint

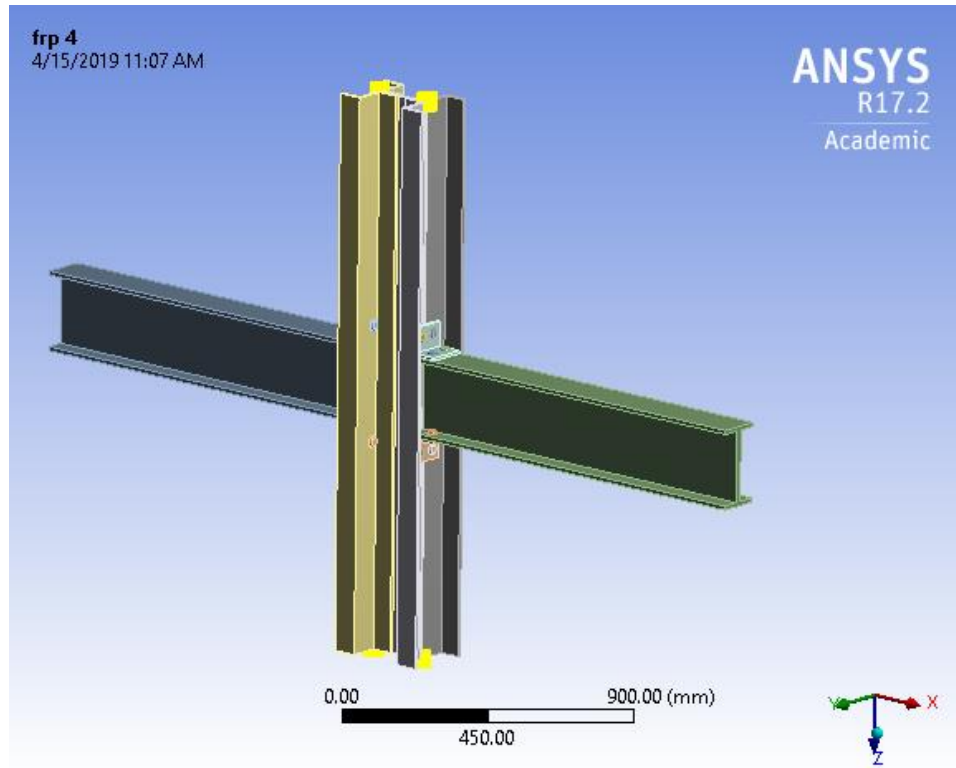


Figure 44. ANSYS model of beam-column connection

#### 4.4.2. Geometry and Material Properties

Two non-retrofitted models with two different concrete properties was used. They are designated as C1 (concrete-encased beam-column connection with 2ksi (13.79 MPa) strength concrete) and C2 (typical C1 with 4ksi (27.598 MPa) concrete). The material properties of the structural steel and rivets were defined as an elastic-plastic material with exact properties discussed in Section 4.4.1. The elastic linear property of the concrete used is provided in Table 4. The strength of the concrete encasement is necessary to evaluate the total strength of the connection. The clear cover of 25-mm and 40-mm is provided to the beam and column respectively for the concrete encasement. The linear property of the concrete in C1 specimen is provided in Figure 45. “Multilinear Isotropic Hardening” property is assigned that defines the stress-strain behavior of

the concrete up to crushing. Figure 46 shows the multilinear isotropic stress-strain diagram of unconfined concrete used in the model analysis using the equation expressed by MacGregor (1992). According to ACI 318-14, the tensile strength of concrete in flexure was defined as 1.73 MPa, which is given by the equation (1). The steel model was defined as the same element type as mentioned in Section 4.4.1, while the concrete cylinder was modeled as SOLID185 element.

$$f_r = 7.5 * \lambda * \sqrt{f_c'} \quad (1)$$

Table 4. Material Properties of Concrete

Specimen	Compressive Strength (MPa)	Tensile Ultimate Strength (MPa)	Modulus of Elasticity (MPa)
C1	13.79	1.73	17875
C2	27.579	2.45	24908

Properties of Outline Row 3: encased concrete			
	A	B	C
1	Property	Value	Unit
2	Density	2322.7	kg m <sup>-3</sup>
3	Isotropic Elasticity		
4	Derive from	Young's Modulus an...	
5	Young's Modulus	17875	MPa
6	Poisson's Ratio	0.19	
7	Bulk Modulus	9.6101E+09	Pa
8	Shear Modulus	7.5104E+09	Pa
9	Uniaxial Compression Test Data	Tabular	
13	Multilinear Isotropic Hardening	Tabular	
14	Scale	1	
15	Offset	0	MPa
16	Tensile Ultimate Strength	1.7344	MPa
17	Compressive Ultimate Strength	13.79	MPa

Figure 45. Linear material property for concrete model of C1 specimen

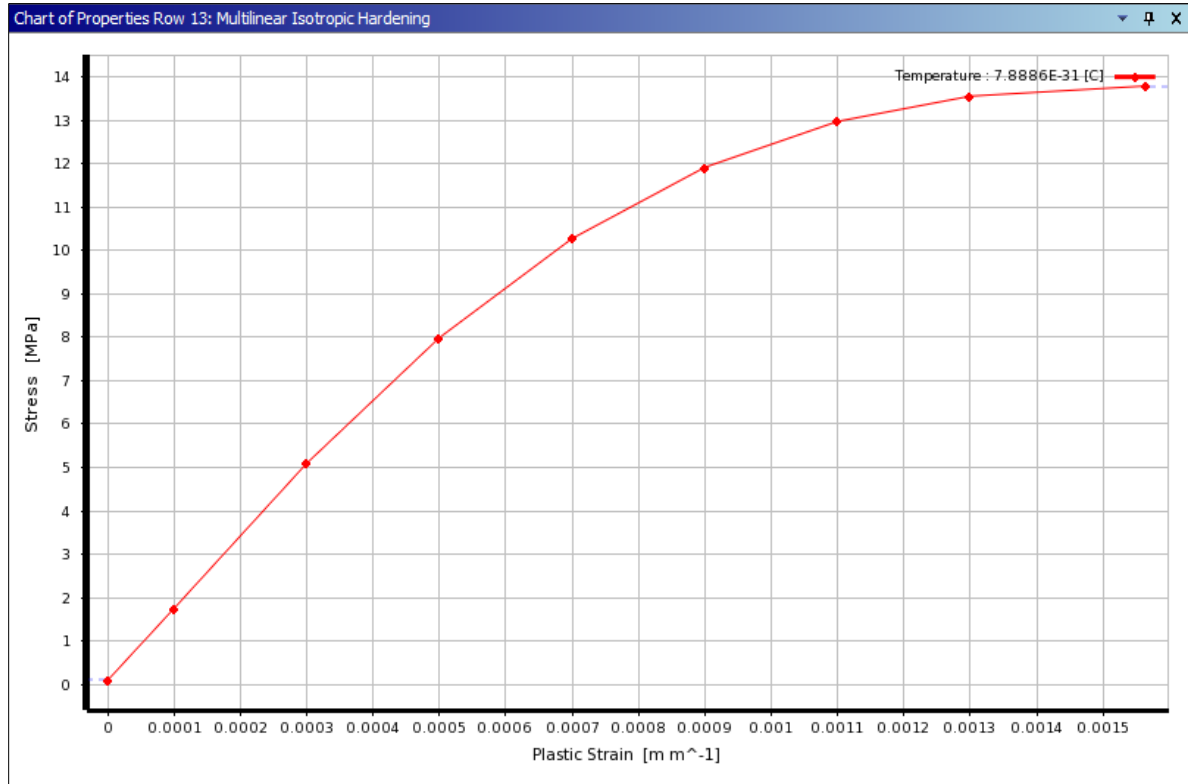


Figure 46. Stress-strain graph of concrete of C1 specimen used in ANSYS according to MacGregor (1992)

#### 4.4.3. Finite Element Idealization of the Connection

The concrete-encased beam-column connection was modeled using Design Modeler to obtain the same model as shown in Figure 39. The finite element model of the connection from the ANSYS file is shown in Figure 47. The boundary condition for the connection model is considered according to the guidelines for cyclic seismic testing of steel structures to obtain the hysteresis behavior of connection. Though the cyclic loading history is not applied to the model, the arrangement used is the test setup for the cyclic loading test. The ends of the extended beams were pinned and a monotonic load in the form of displacement-controlled loading was applied to the column axially. This is an indirect way of obtaining the same behavior as when beam tip is loaded.

The load applied on the column will be balanced by the reaction force on the pinned ends of the beams, which is then multiplied with the length of the extended beam to obtain the moment capacity of the connection. The displacement of the nodes at the tip of the beam was measured using DISPLACEMENT PROBE as a part of the solution. The obtained displacement data was transformed into rotation for each side of the column and the obtained moment-rotation curve is plotted in Figure 50. In addition, the plot of displacement that the entire system endured against the load was produced to evaluate the load carrying capacity of the joint, which is shown in Figure 49. The concrete cylinders are in “BONDED” contact with the steel. To ensure the mesh convergence, the model was meshed with coarser mesh and reducing the element size until getting the closer results. The process resulted to an 80 mm quadratic element size using “HEX DOMINANT METHOD” for meshing and the meshed model is shown in Figure 48.

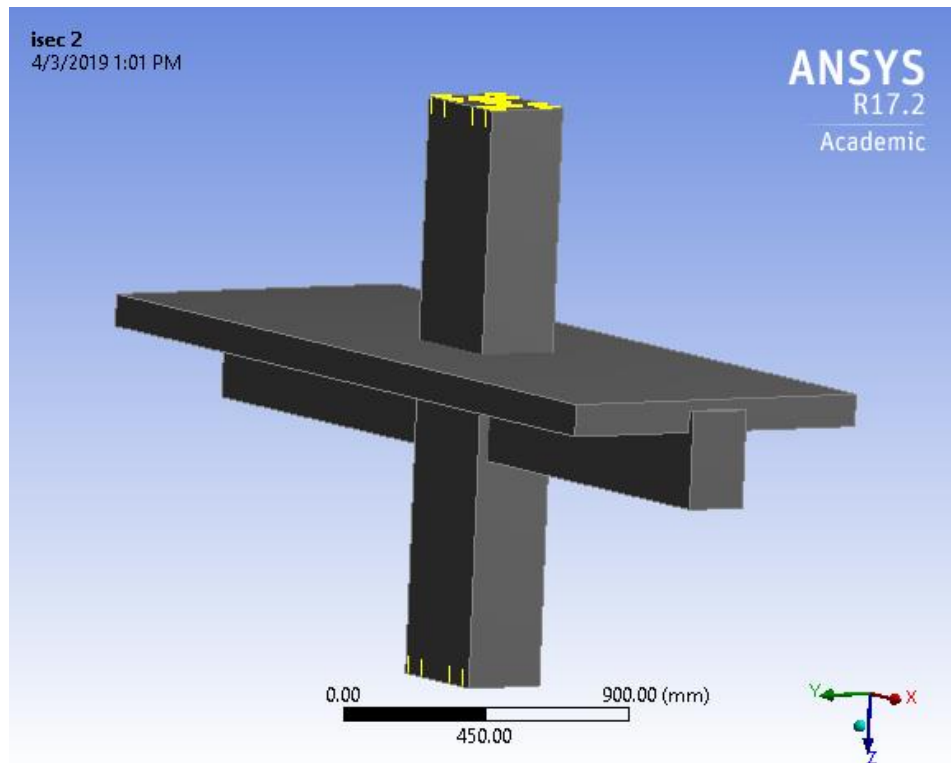


Figure 47. ANSYS model (Concrete-encased beam-column connection)

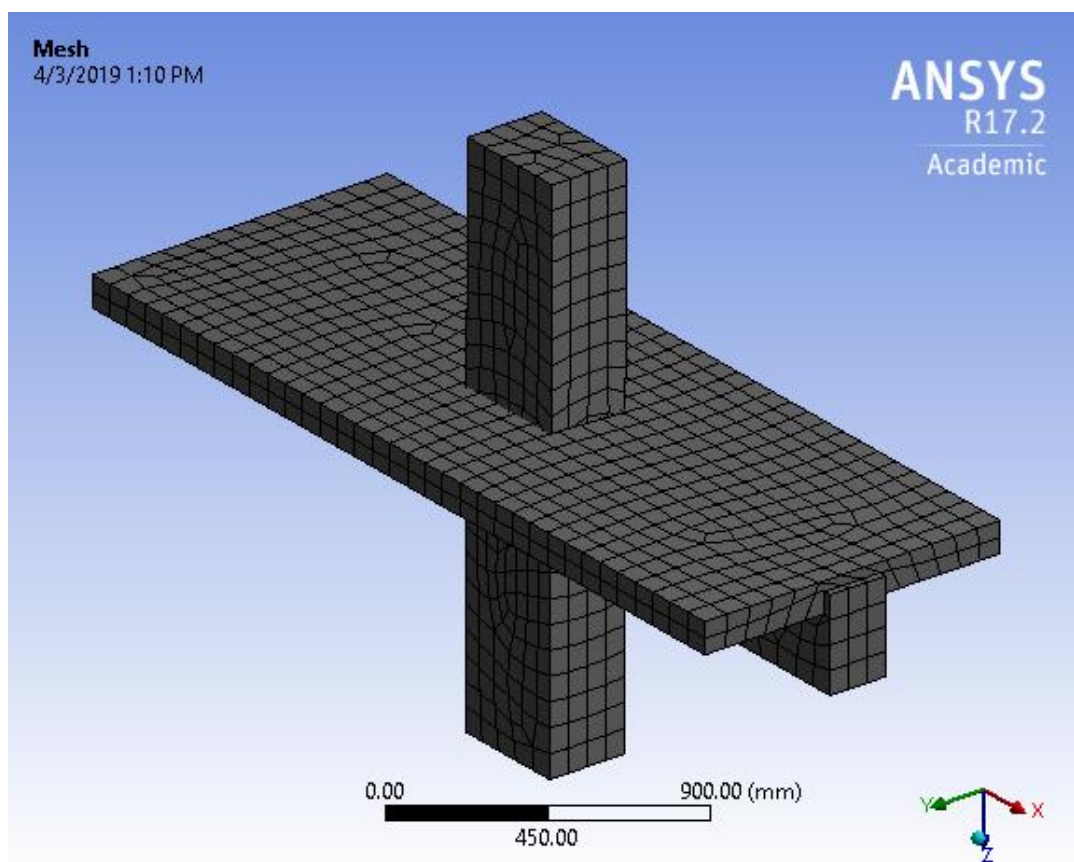


Figure 48. Meshed model (Concrete-encased beam-column connection)

#### 4.4.4. Analysis Results

Two different load patterns were applied to the model: (i) load applied axially in the positive Z-direction and (ii) negative Z-direction. The final moment rotation (M- $\theta$ ) curve obtained from the analysis is shown in Figure 50 and the load deformation curve is shown in Figure 49. Since both the beams of the connection is identical, the M- $\theta$  relationship is plotted for only one side of the column. From the graphs, the maximum load carrying capacity of the control specimen C1 when loaded in negative Z direction is obtained to be 598kN and when loaded in positive Z direction is 534kN. The maximum load value for C2 specimen is obtained 704kN in positive Z and 790kN in



negative Z direction. Similarly, the C1 connection has developed the maximum moment of 359kNm at a rotation of 0.01038 radian and 320kNm at a rotation of 0.008 radian when loaded in negative and positive Z direction respectively. The moment capacity of connection with higher strength concrete was found to be 426kNm at rotation of 0.0086 radian and 477kNm at a rotation of 0.0102 radian in positive and negative Z direction respectively. When concrete of 4ksi strength was used for the encasement, the load and moment capacity of the connection increased by 31% and 32% respectively in positive and negative Z direction. The graph below clearly shows the increase in load carrying and moment capacity of the connection with the increase in strength of concrete encasement.

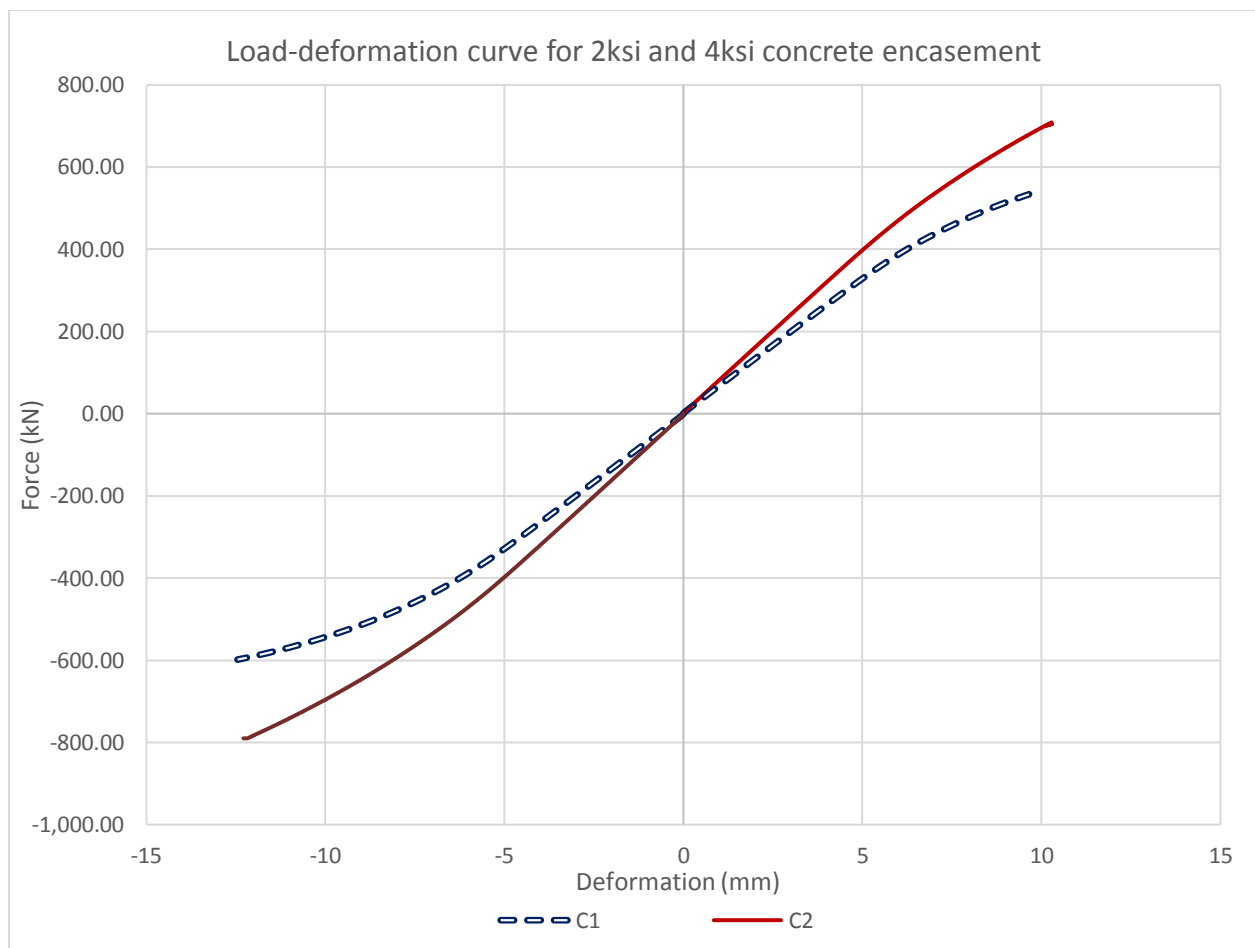


Figure 49. Load-displacement graph of concrete-encased control specimens

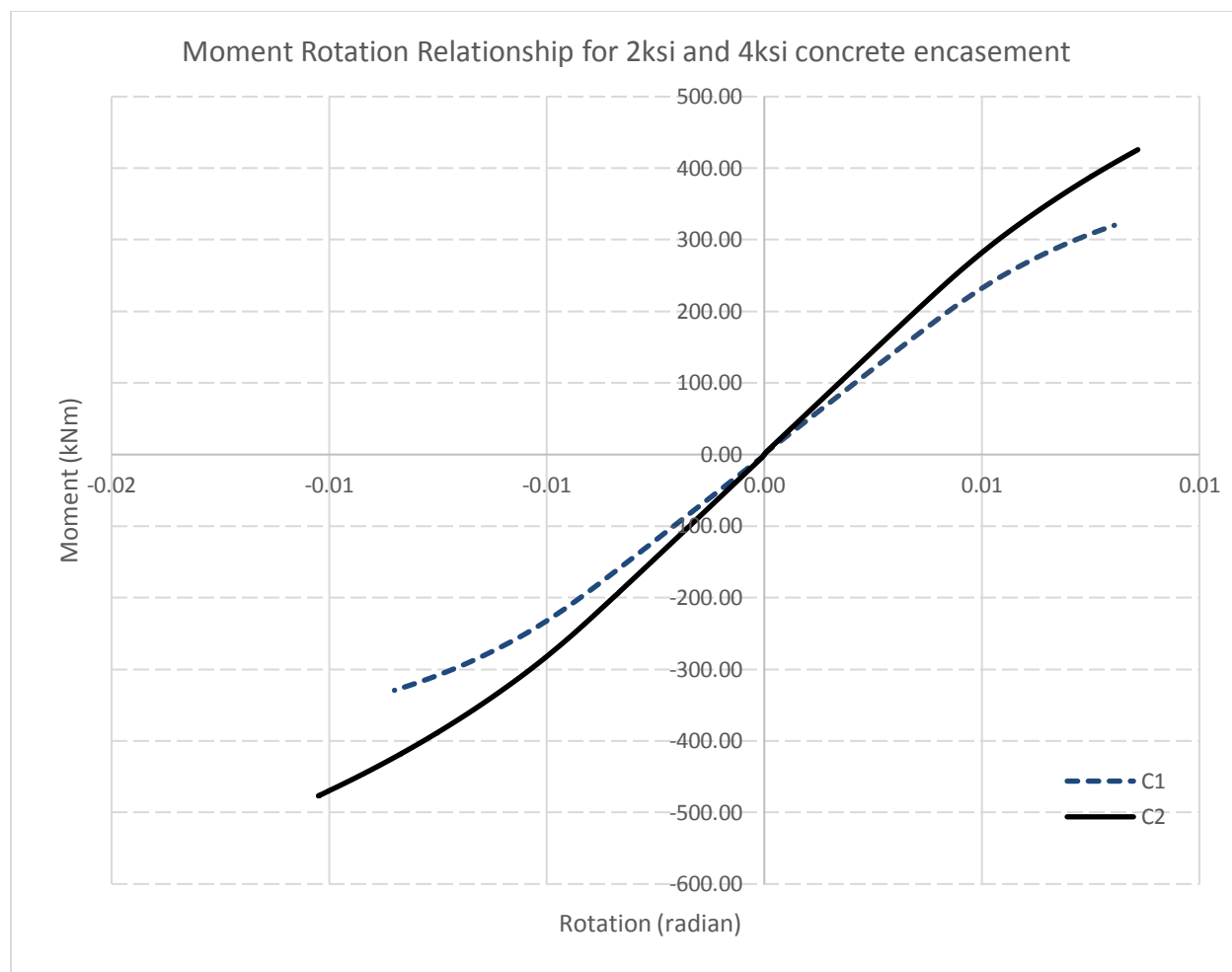


Figure 50. Moment-rotation curve of concrete-encased models

#### 4.5. Finite Element Modeling of Behavior of Retrofitted Concrete-Encased Connection

In this section, the study of the behavior of the FRP retrofitted concrete-encased beam-column connection was done. The finite element analysis of the retrofitted connection was performed to study the moment rotation relationship of the beam-column joint. The details of the configuration of FRP used in the analysis is considered from the drawing produced by FYFE company for beam, column and slab strengthening as given in Figure 1. FYFE designs and manufactures TYFO® FRP system for strengthening of the structures.

In this project, three different retrofitted models with different types of FRP application was considered and analyzed to observe the change in load and moment carrying capacity of the connection. The three retrofitted models were designated as T1, T2 and T3 and their respective FRP configuration is described in Table 5. The cross-section details of one of the specimens is shown in Figure 51.

Table 5. Description of Models used in Finite Element Analysis

<b>Specimen Designation</b>	<b>Retrofit Scheme</b>
C1	Control Specimen (Non-retrofitted concrete encased connection with 13.79 MPa concrete)
C2	Typical C1 with concrete encasement of 27.579 MPa concrete.
T1	One layer of TYFO SCH-41 wrapped around column 2 foot height from face of column, one layer of FRP sheet vertically oriented to beam face and a typical 1-foot strip laid on the slab in 2 layers.
T2	One layer of TYFO SCH-41 2X wrapped around column 2 foot height from face of column, one layer of same sheet vertically oriented to beam face and a typical 1-foot strip of TYFO SCH-41 laid on the slab in 2 layers.
T3	Typical T1 but with higher strength concrete encasement (27.579 MPa)

#### 4.5.1. Geometry and Material Properties

The material properties of the structural steel and rivets were defined in Section 4.4.1. The concrete linear and non-linear properties were adopted the same as discussed in Section 4.4.2. The concrete cylinders and structural steel elements were designated as SOLID185 element while the rivets were modeled as SOLID285 element. The fiber reinforced polymer (TYFO® system) consists of epoxy matrix and reinforcing dry fibers whose combination makes a monolithic composite material. It is a unidirectional carbon fabric oriented in the 0° direction, the material properties of which is provided in Table 6. The material properties were obtained from the data sheet in the catalogue of each FRP composite available in the FYFE company website. The FRPs were assumed to show linear elastic behavior till rupture. The value for Young's modulus in the hoop

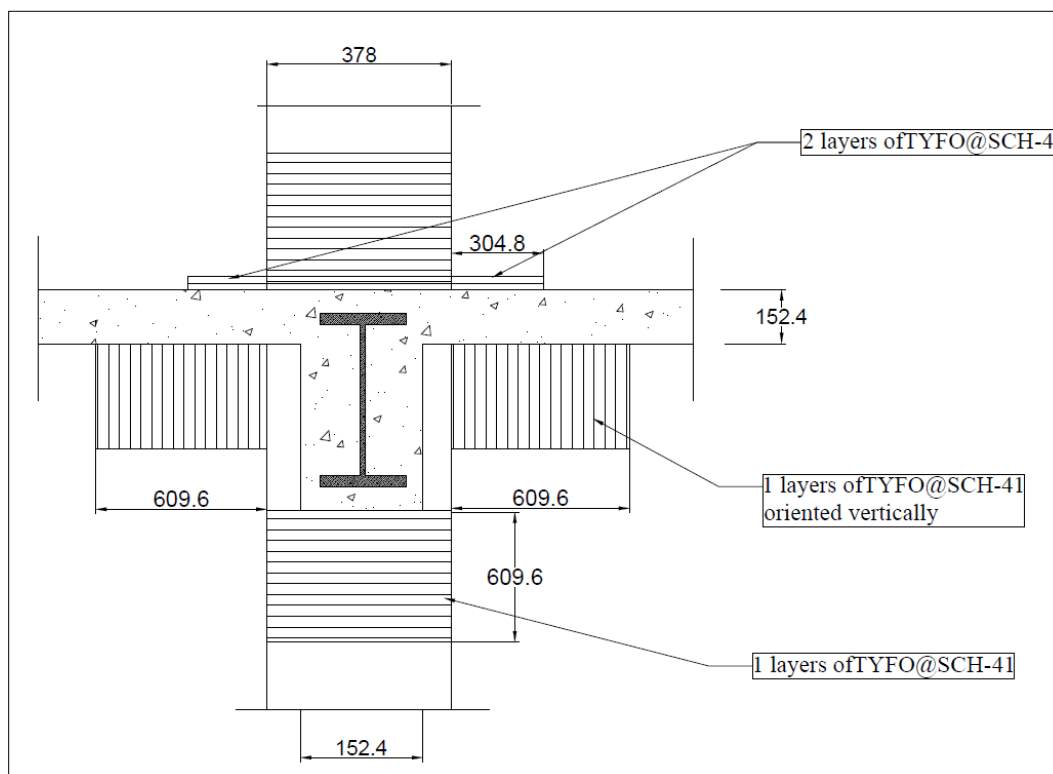


Figure 51. Cross-section details of retrofitted connection (T1 specimen)

direction was defined with the value given by the manufacturer whereas the value of modulus of elasticity and shear modulus in other direction were assigned small values as shown in Figure 52. The FRP sheets were modeled as a thin lamina using an eight-node homogenous element having three degree of freedom at each node, SOLID185.

Table 6. Material Properties of FRP (obtained from FYFE catalogue)

	Tensile Strength (MPa)	Modulus of Elasticity (GPa)	Thickness (mm)
TYFO SCH-41	986	95.8	1.0
TYFO SCH -41 2X	986	95.8	2.0

	A	B	C
1	Property	Value	Unit
2	Density	1771.5	kg m <sup>-3</sup>
3	Orthotropic Elasticity		
4	Young's Modulus X direction	95837	MPa
5	Young's Modulus Y direction	123.42	MPa
6	Young's Modulus Z direction	123.42	MPa
7	Poisson's Ratio XY	0.2	
8	Poisson's Ratio YZ	0.02	
9	Poisson's Ratio XZ	0.02	
10	Shear Modulus XY	79	MPa
11	Shear Modulus YZ	79	MPa
12	Shear Modulus XZ	79	MPa
13	Tensile Ultimate Strength	986	MPa
14	Compressive Ultimate Strength	86	MPa

Figure 52. Orthotropic elasticity material property of FRP

#### 4.5.2. Finite Element Idealization of the model

The retrofitted model of concrete-encased beam-column connection was modeled using Design Modeler to obtain the model as shown in Figure 53. The boundary condition for the connection model is the same as discussed in Section 4.4.3, which is pinned supports at beam ends and axial loading of the column to obtain the same behavior as when beam tip is loaded. This is the standard boundary condition guidelines for cyclic seismic testing of steel structures as per Guideline ATC 24 (1992). The rotation of the nodes at the tip of the beam was calculated using the displacement data of the displacement of node at the beam end using an ANSYS “DEFORMATION PROBE” as a part of solution. The obtained values were used to produce the moment-rotation curve, which is plotted in Figure 57. The contact defined for steel and concrete remains the same as discussed in previous section 4.4.3. A perfect bond between the encased concrete and the FRP sheets was assumed. The steel model and concrete model is meshed with an 80 mm quadratic element size using “HEX DOMINANT METHOD”. The mesh convergence was considered while coming up with the adopted element size in the analysis. The meshed model is shown in Figure 54.

#### 4.5.3. Analysis Results

As discussed in previous section 4.4.4, similar load pattern was applied to the retrofitted model as well. The positive and negative Z-direction axial load was applied to the models with all three FRP configurations as discussed in previous section. The deformed shape of the retrofitted model T1 is shown in Figure 55. A load-deformation graph and the moment rotation curve obtained from the analysis for models T1, T2 and T3, when loaded in positive and negative Z direction is shown in Figure 56 and Figure 57, respectively. The numerical values of the graph are represented in Table 7 for clear understanding and comparison. From the figures 49 and 50, and the graphs and table

below, it can be seen that the maximum load carrying capacity and the moment capacity of the retrofitted connection is more than the non-retrofitted model. Also, the load and moment capacity of the retrofitted models increased with increasing thickness and number of layers of FRP used.

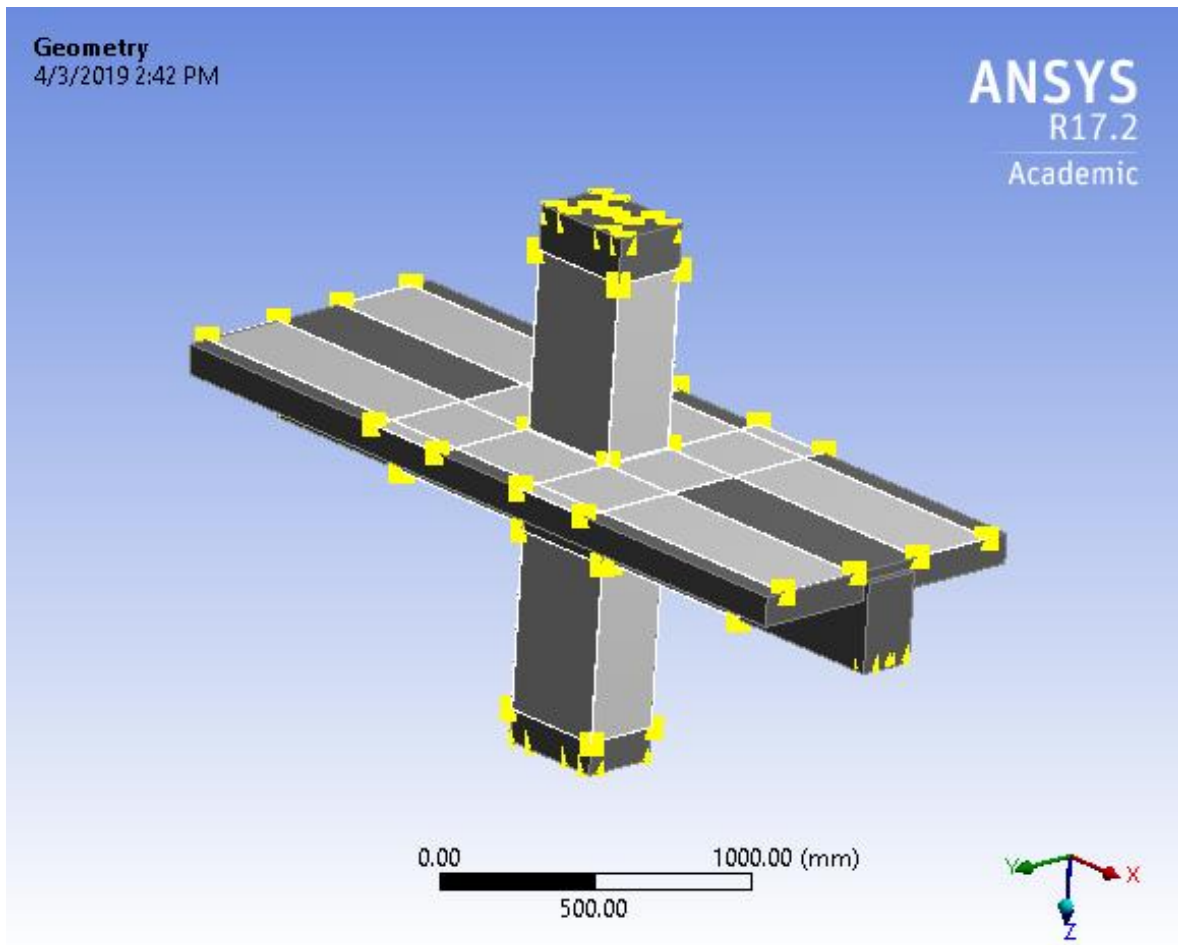


Figure 53. ANSYS model of retrofitted concrete-encased beam-column connection

Table 7. Finite Element Analysis Result for Retrofitted Specimen

Specimen	Loading in +Z-direction		Loading in -Z- direction	
	Load capacity (kN)	Moment capacity (kNm)	Load capacity (kN)	Moment capacity (kNm)
T1	668	401	656	393
T2	708	425	668	401
T3	876	526	864	518

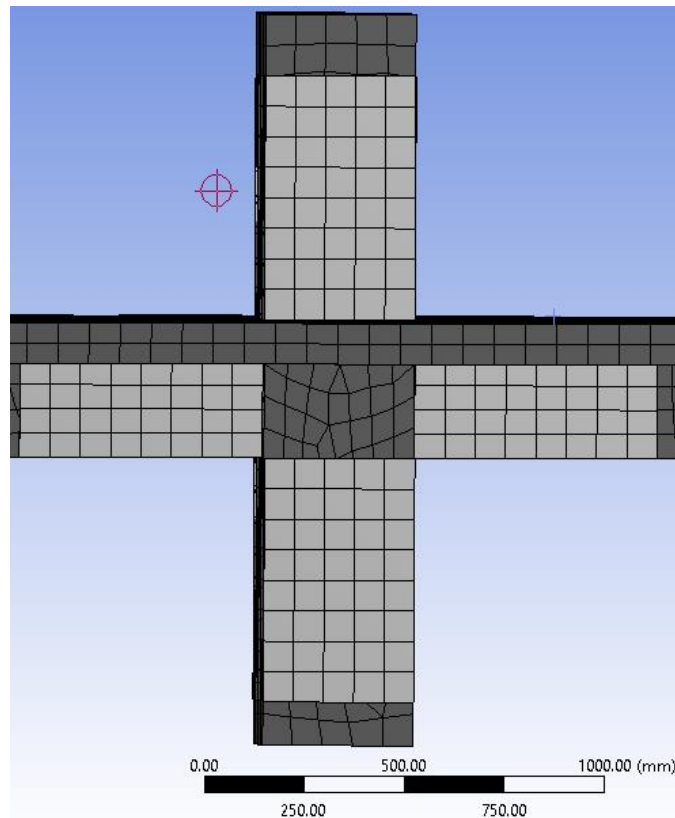


Figure 54. Meshed Model of Retrofitted Beam-column connection



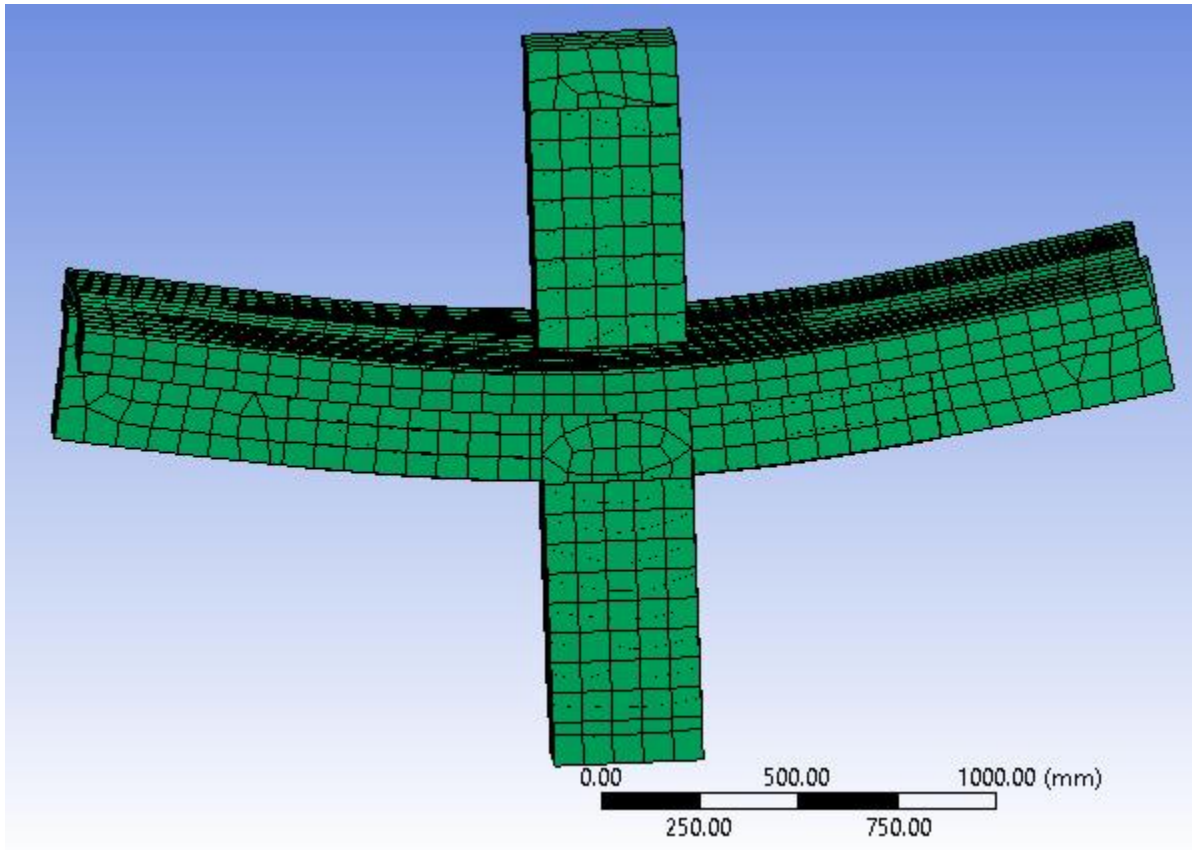


Figure 55. Deformed Shape of Retrofitted Model T3 (loading in +Z direction)

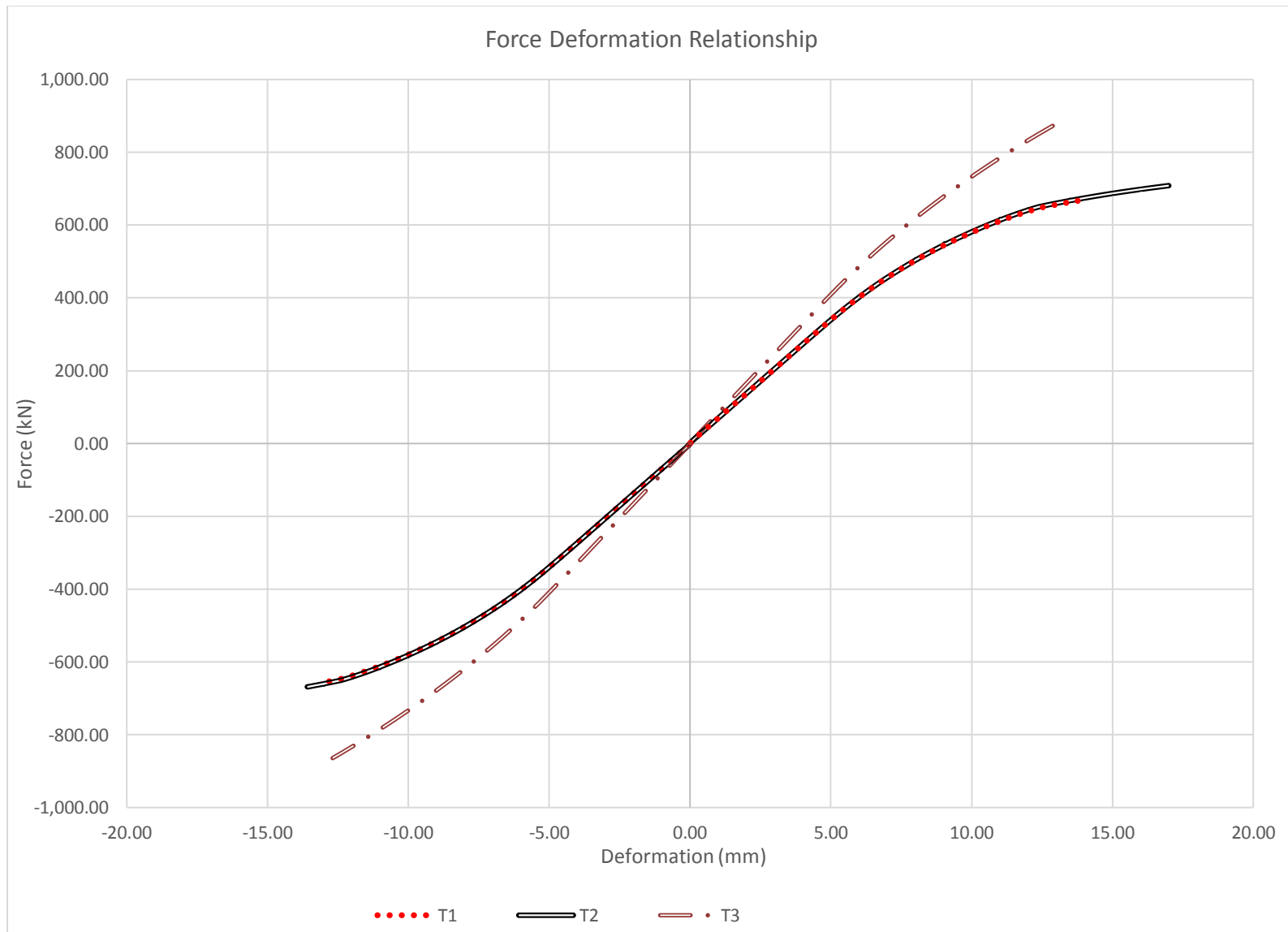


Figure 56. Load-displacement curve of retrofitted specimens T1, T2 and T3

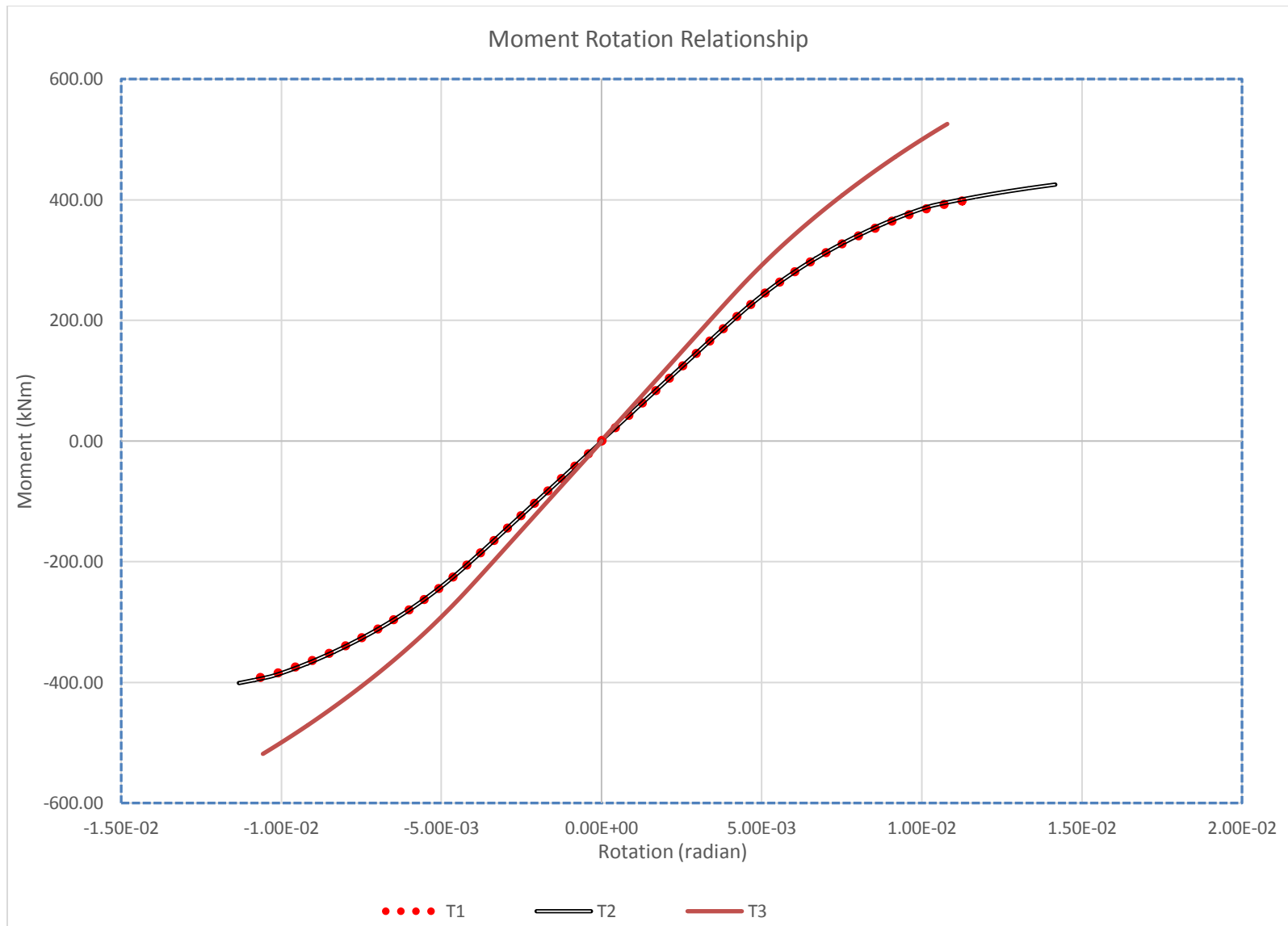


Figure 57. Moment-rotation curve of retrofitted models T1, T2 and T3

## CHAPTER V. COMPARISON AND DISCUSSION OF RESULTS

### 5.1. Comparison of Retrofitted and Non-Retrofitted Connection

The finite element analysis has been performed on the plain non-retrofitted specimens (C1& C2) and retrofitted specimens (T1, T2 & T3) with different FRP configurations as described in Table 5 to obtain the load deformation and moment rotation behavior of the connection. The load-deformation curve and moment rotation curve obtained for both the plain and retrofitted specimens has been superimposed in Figure 59 and Figure 60 to make comparison of the results. As it is already discussed in the result section for control specimens, the moment connection has developed high load carrying capacity and moment resistance when a higher strength of concrete encasement is provided to the steel frame. It can also be explicitly seen from the figure that the retrofitted specimen has increased load carrying capacity and moment capacity than the plain specimen. The results also indicate the increased initial slope and stiffness of the retrofitted specimen compared to the non-retrofitted one. It is important to mention that the end points where the plotted curve ends, represents the instability failure of the model due to abrupt separation of contact surfaces and distortion found in element of model due to high stress concentration. The finite element model failed to converge beyond this point due to the distortion of elements.

Comparing the yielding point of control specimen C1 and retrofitted model T1, the first yielding for plain model occurs at 350kN with displacement equal to 5.3 mm. However, for the retrofitted specimen T1, the first yielding occurs at 375kN with displacement equal to 5.64 mm. The increase in the yield load and displacement in which the yielding occurred are about 6.4 and 7.1 percent

respectively. The use of FRP sheets have shifted the yielding of the model and has improved the behavior of the joint.

The moment capacity of the non-retrofitted connections C1 and C2 was obtained as 359kNm and 477kNm in negative Z direction, whereas 320kNm and 426kNm when loaded in positive Z direction respectively. Since we have used steel beam W8x35 ( $Z_x=34.7 \text{ in}^3$ ) with yield strength of 28000 psi in the connection, we can numerically evaluate the moment capacity of the steel beam using Equation (2). The moment capacity of the beam itself was calculated to be 971600 lb-in (110kNm), which is smaller than the obtained moment of 359kNm for the concrete encased beam. The concrete encasement has added to the additional moment capacity of the concrete-encased steel beam.

$$M_p = F_y * Z_x \quad (2)$$

The extracted results from ANSYS for the load capacity and moment capacity of the retrofitted model (presented in Table 7) is compared against the plain non-retrofitted models and the final comparison is showed in Table 8. From the table below, it can be evaluated that the retrofitted specimen T1 and T2 has increased moment capacity than the plain model C1 by 25% and 33% respectively in positive Z direction. Similarly, when loading is applied in negative Z direction, the specimen T1 and T2 has enhanced moment capacity of 9% and 12% more than the moment capacity of the non-retrofitted specimen C1. Comparing the specimen C2 and T3 also shows 24% and 9% increment in load carrying capacity and 23% and 8.6% increment in moment capacity in respective positive and negative Z direction. Similar type comparison is done between the retrofitted and non-retrofitted models with varying concrete strength in Figure 61 and Figure 62. The graph clearly proves that the strength of the connection for the models with 4ki concrete

showed enhancement in load and moment capacity than the models using 2ksi concrete. To be precise, the load and moment capacity of C2 is higher than C1 and likewise T3 showed increased strength than T1 regardless of same FRP configuration. The displacement value which the system can endure was also increased due to the FRP retrofitting. It is important to note that the retrofitted system showed substantial increment in load carrying and moment carrying capacity of the connection when loaded in positive Z direction, however the enhancement in the negative Z direction looks minor. The reason could be the increased stiffness in the direction of loading in negative Z direction due to heavy weight slab.

Table 8. Comparison of Plain and Retrofitted Model Capacity

Specimen	Loading in +Z-direction		Loading in -Z- direction	
	Load capacity (kN)	Moment capacity (kNm)	Load capacity (kN)	Moment capacity (kNm)
C1	534	320	598	354
C2	704	426	790	477
T1	668	401	656	393
T2	708	425	668	401
T3	876	526	864	518

In addition to the evaluation of the moment capacity, the finite element results for the maximum principal stresses obtained in the non-retrofitted and retrofitted model was analyzed to check if there was any shift in the location of maximum stress from the face of the column. The location of formation of the maximum principal stress was only compared among C1, T1 and T2 specimens (with 2ksi concrete) to visually interpret the outcome of retrofitting. When loaded in negative Z-direction, the maximum principal stress in the connection was found to occur at the flange of the beam, which was almost at 250mm, 300mm and 350mm away from the column face, respectively, for C1, T1 and T2 specimen. The figures representing the maximum principal stress is shown in Figure 58.

Likewise, when loading in positive Z direction, the maximum principal stress in the C1 specimen occurred very near to the face of the column, 50mm distant from column face. The location at which the maximum principal stresses occurred for T1, and T2 specimen was 185 mm, and 200mm from the face of the column as shown in

Figure 63. It can be concluded that the use of FRP retrofitting not only increases the load and moment capacity of the connection, but also helps in shifting the location of maximum principal stress away from the face of the column.

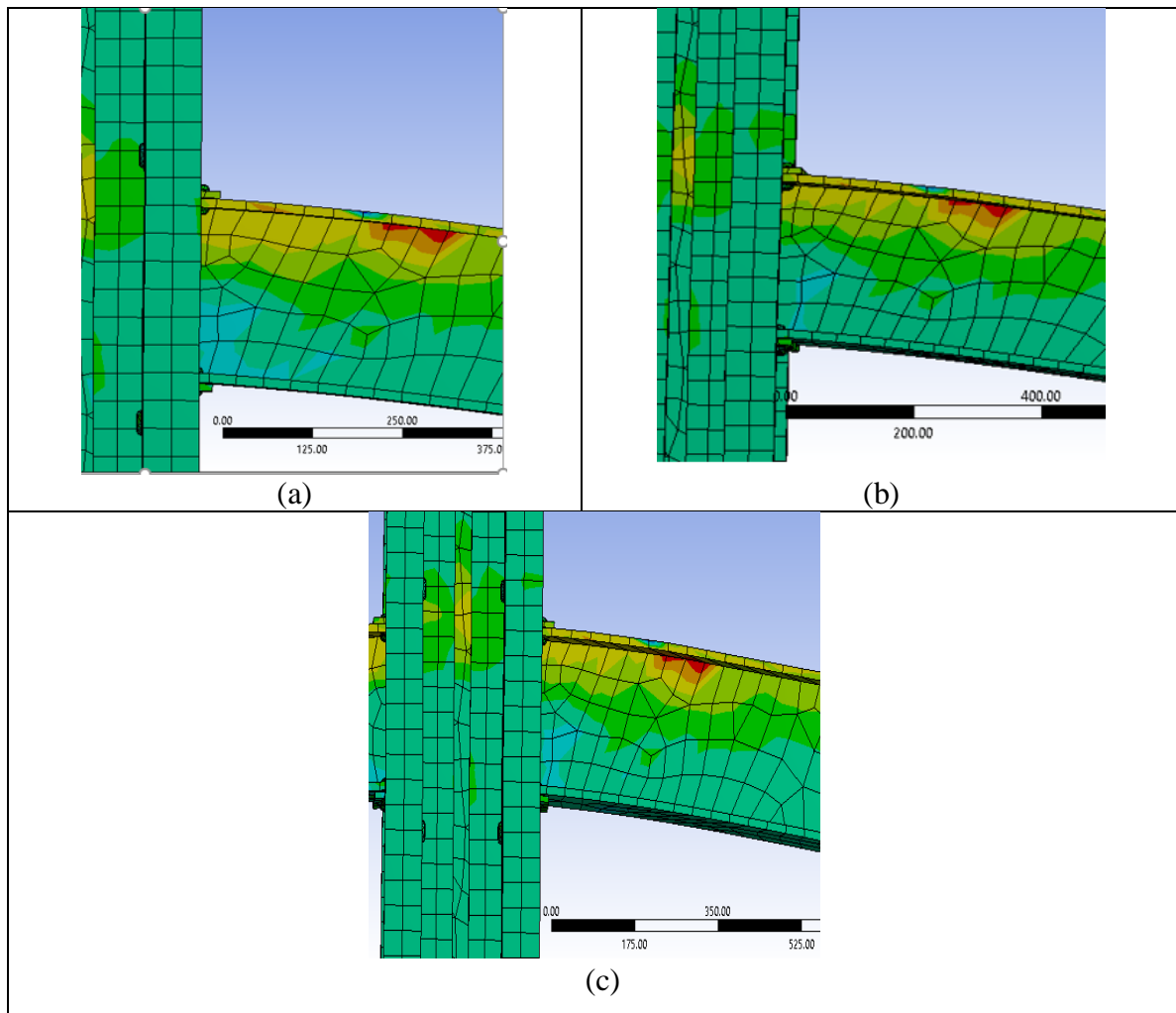


Figure 58. Maximum principal stress in; (a) C1 specimen; (b) T1 specimen; (c) T2 specimen

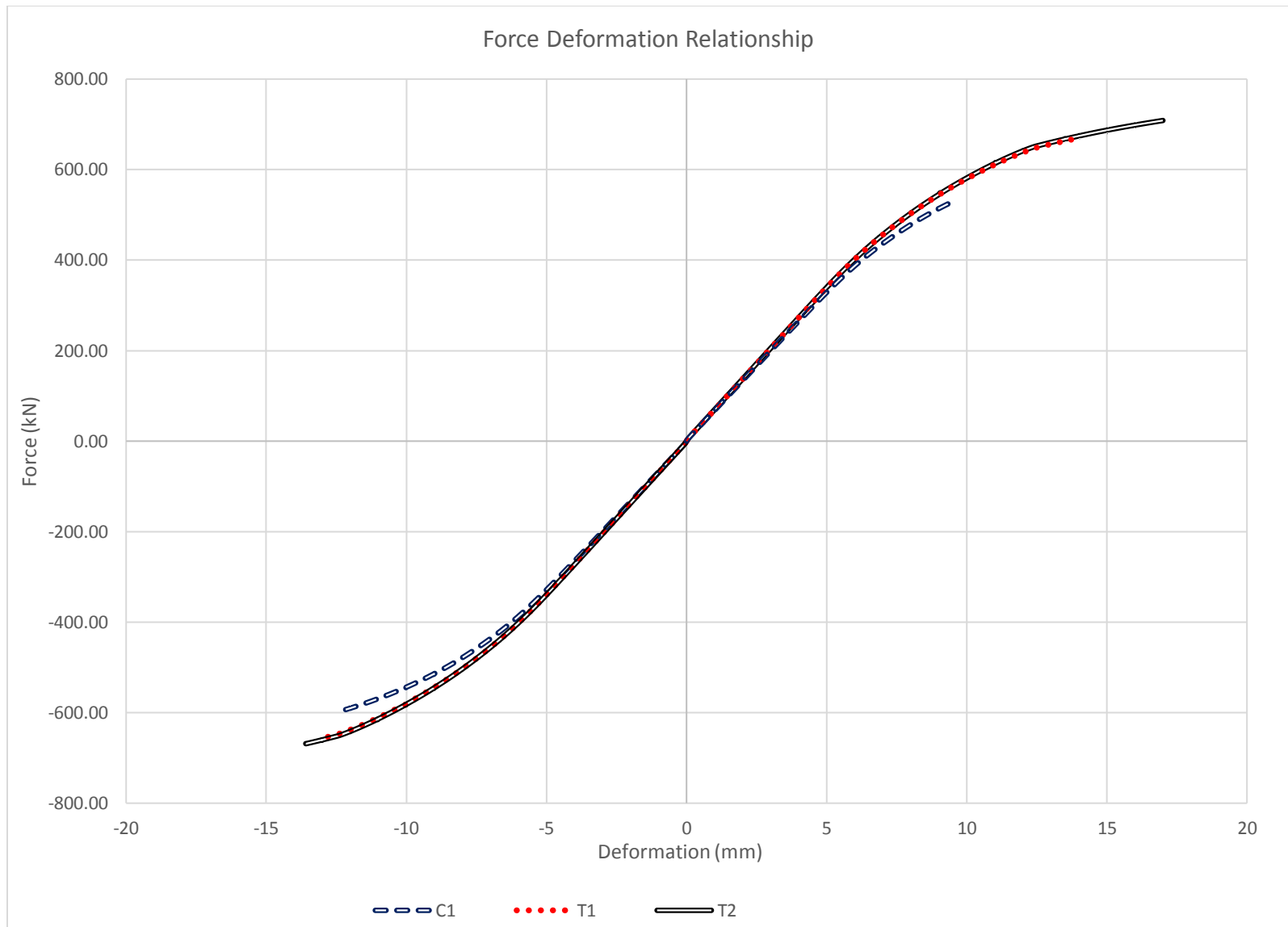


Figure 59. Comparison of load displacement graph (Non-retrofitted v/s retrofitted) using 2ksi concrete



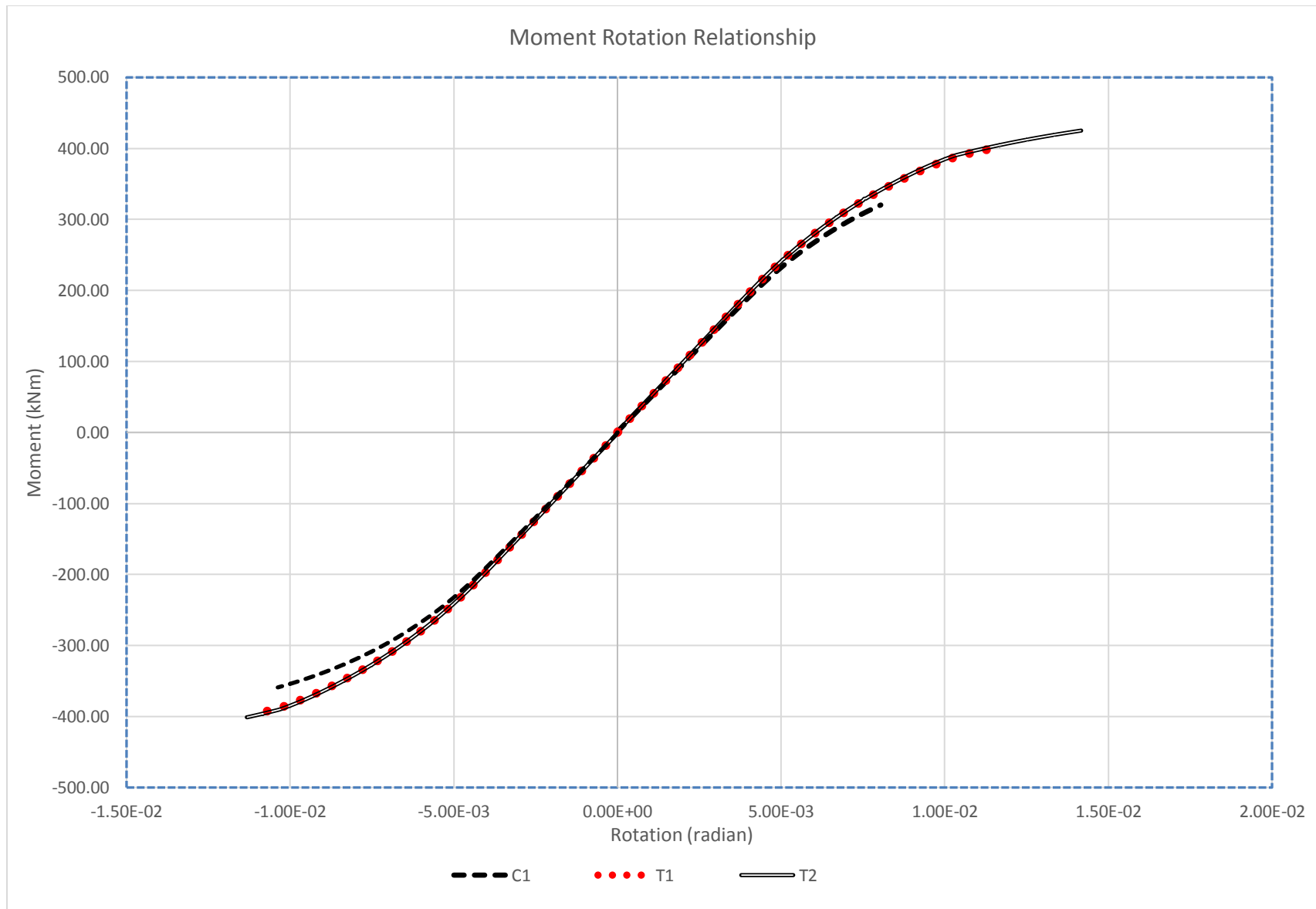


Figure 60. Comparison of moment rotation curve for plain and retrofitted specimens with 2ksi concrete

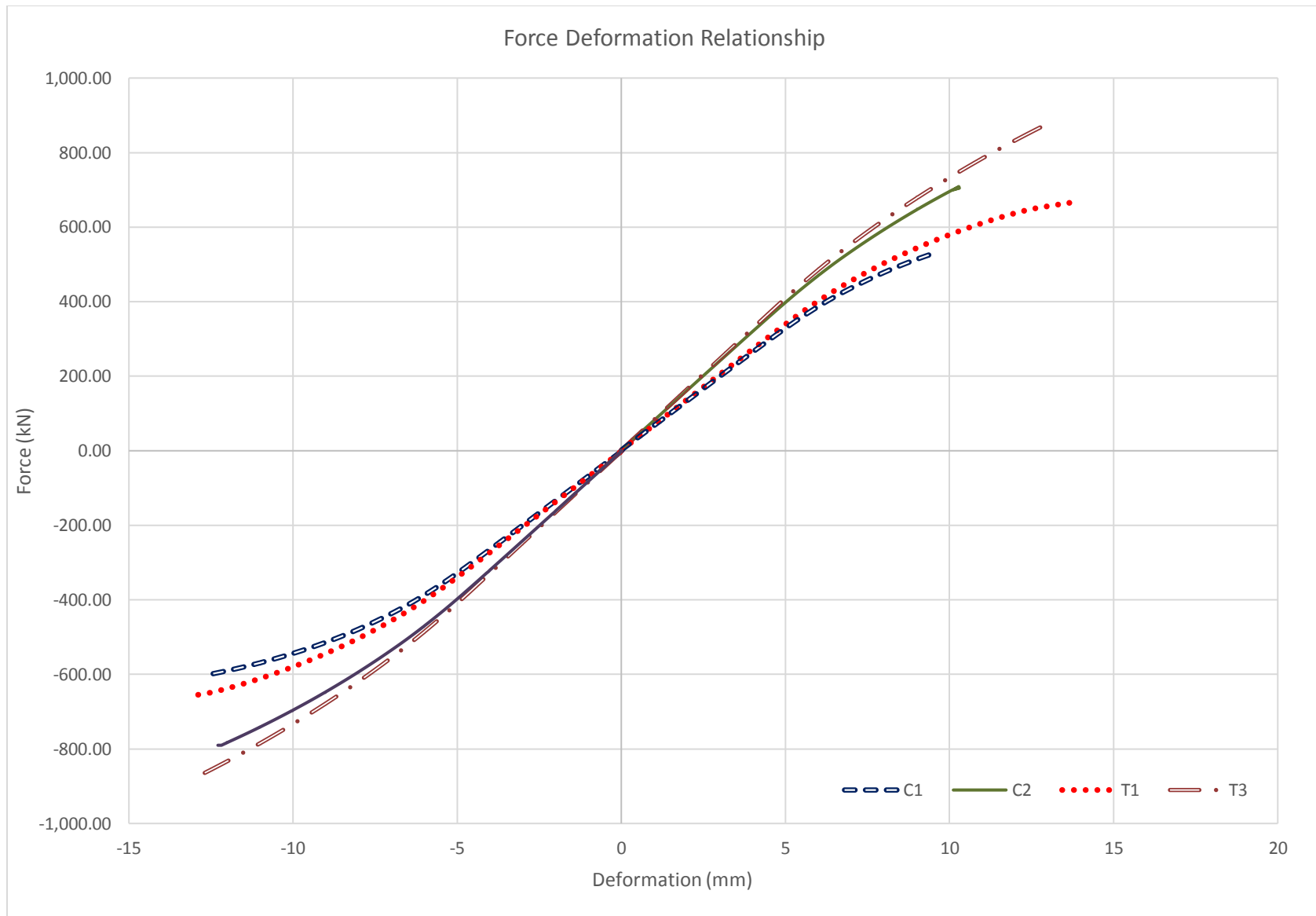


Figure 61. Comparison of load deformation curve for plain and retrofitted specimens

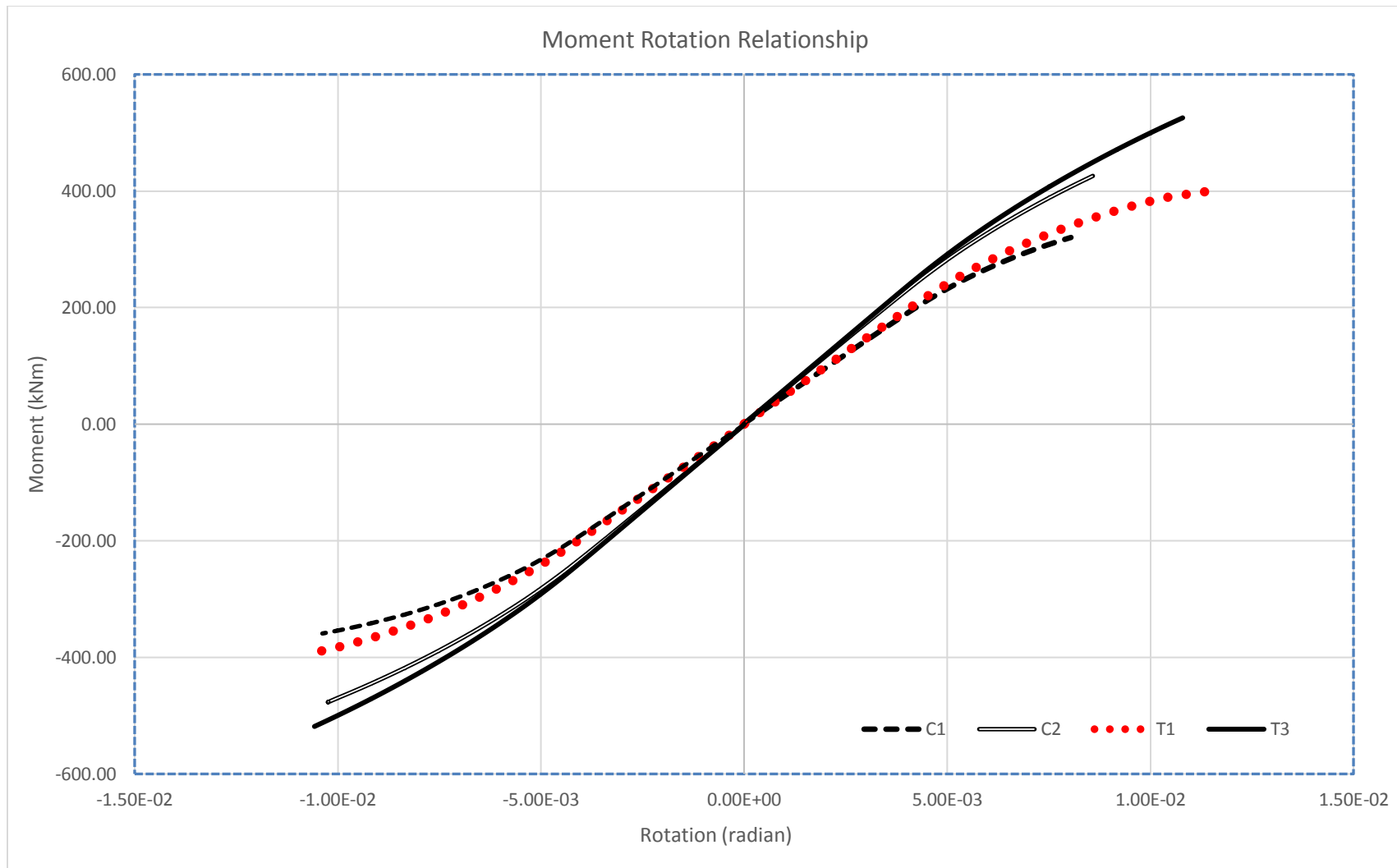


Figure 62. Comparison of moment rotation curve for plain and retrofitted specimens

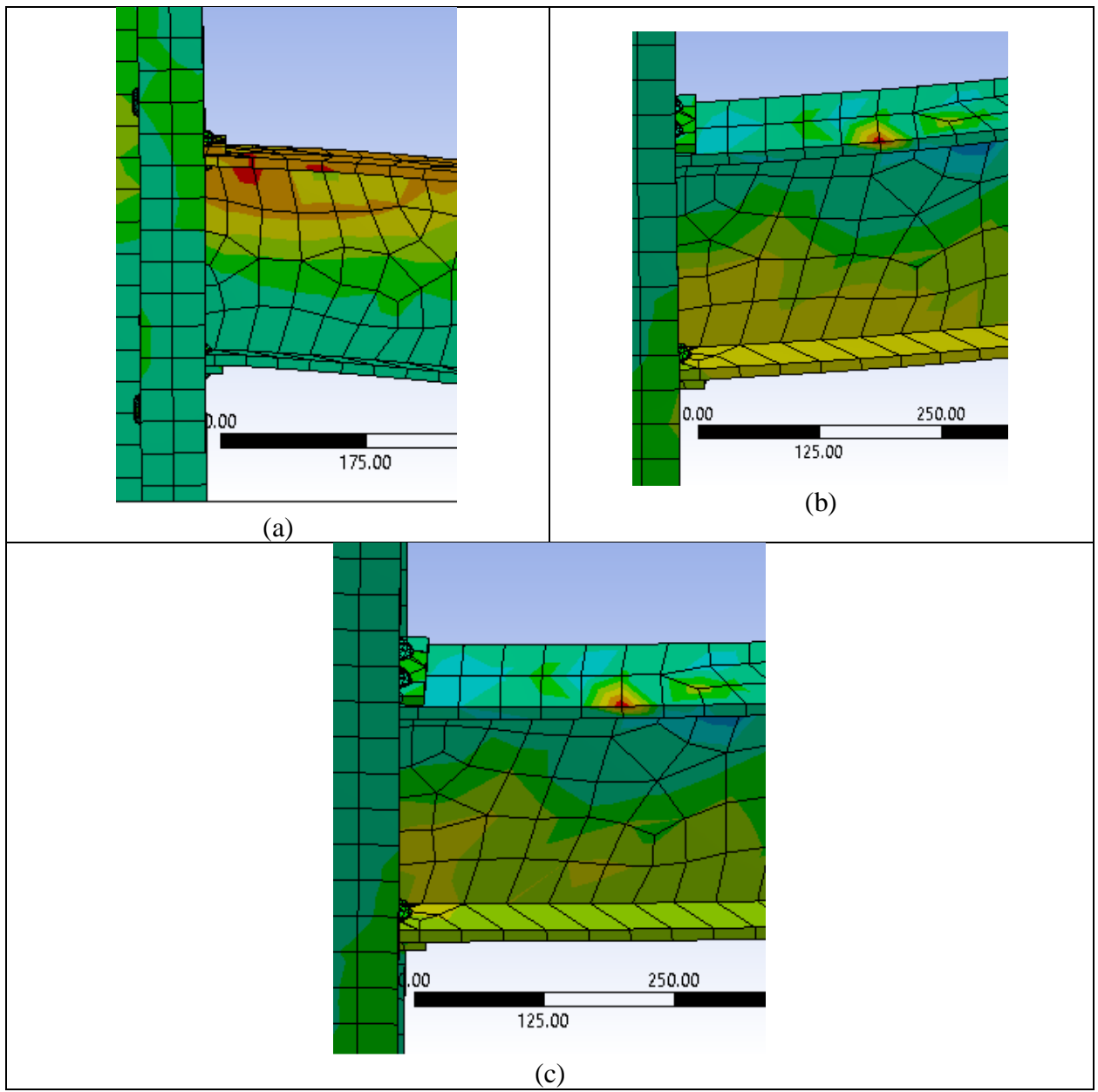


Figure 63. Maximum principal stress in; (a) C1 specimen; (b) T1 specimen; (c) T2 specimen

From the general observation, the use of FRP retrofitting in the specimen has affected the behavior of the connection. Comparison of the results obtained from the finite element analysis on the control specimen C1 and C2, and the retrofitted specimens (T1, T2 and T3) indicate that the FRP retrofitting technique used in the research has increased the load, displacement and moment

carrying capacity of the connection, however, it also makes the connection more rigid by increasing the overall stiffness of the system. It was also observed that by increasing the thickness of the FRP layer and adding an additional layer of FRP to the system, the load and moment capacity of the connection was increased remarkably. There was also found the shift in formation of plastic hinge by increasing the thickness of FRP and adding layer of FRP in the system. The strength of concrete encasement also seems to affect the performance of the joint remarkably. When concrete of 4ksi strength was used for the encasement, the load and moment capacity of the connection increased nearly by 34% and 9% respectively in positive and negative Z direction. This project only considered using the FRP configuration provided in FYFE drawing (Figure 1) and it could be possible that some other type of configuration can yield better performance of the connection, which is proposed in the future works.

## 5.2. Problems Encountered and Limitations

The model considered for the finite element analysis was in itself a complicated model with built-up columns and rivet connections in them. There were many difficulties encountered during modeling and analysis of the connections which are listed below:

- Difficulty in modeling of the connection and rivets.
- Difficulty in meshing of irregular geometry such as rivets and concrete element of the model.
- Non-convergence of the analysis due to non-linearity property and geometry.
- Problems of defining the right properties for concrete model to produce the confined characteristic of the concrete.
- Excessive amount of time required for the solution due to limitations on the processing system of the computers.

Due to the above-mentioned problems encountered, there were some modifications accepted in the model for the analysis:

- The Zee-section was assumed to be a continuous section without introducing rivets along the height of the column. The buckling of column was not considered as an important parameter in the case since it was only the moment capacity of the beam-column connection under investigation.
- The force and displacement convergence tolerance percentage were taken as  $\pm 5\%$ .

### 5.3. Future Work

The research focused on analyzing the behavior of the steel connections, however the connection taken for analysis was not a typical one. The column section was a built up column consisting of Zee-shaped steel sections connected via rivets. Additional information seems required about the cyclic behavior of these type of old riveted connections. The following topics should be considered for further research:

- Finite Element Analysis to obtain the hysteresis behavior of this type of connection, so that it can be used to investigate the seismic behavior of the buildings having similar structural elements.
- Experimental tests on the connection to study the behavior of this type of beam-column connection and predict if the analytical model showed viable results.
- Further investigation on concrete encasement and the effects of confinement in the hysteresis behavior of the connection.
- Further analysis of the model using different configuration of FRP sheets to observe if any other configuration yields better strength.
- Further investigation is required on different types of retrofitting techniques of this kinds of connections other than FRP strengthening.

## CHAPTER VI. CONCLUSION

This research began with the objective of verifying if the use of a particular FRP technique to retrofit the concrete-encased beam-column connection yields better strengthening of the joint for the future. For a real project, the section of the connection was considered from an actual building named The Syndicate, located in St. Louis, Missouri. We had also received a drawing from FYFE including the FRP wrap configuration for strengthening the beam, column and slab. The same configuration and the properties of the FRP as given in the drawing were adopted in the analysis. In addition to the provided configuration, the thickness of the FRP layer was increased and an additional FRP layer was applied to the present settings to compare the changes in the behavior of the retrofitted models. The main objective of the research was to conduct a finite element analysis of the connection (with and without FRP) to compare the results.

During the initial phase of the research, there were some issues with the modeling of the rivets and the contact between the elements to ensure the correct performance of the model. That is why a simple lap joint model was analyzed to verify the behavior of the rivet connection. Similarly, load deformation relationship of a steel column retrofitted with FRP wrap and concrete filling was studied to investigate how to model the concrete and FRP in the finite element model. Owing to the verification of the finite element analysis of both the model with the experimental results, the concrete-encased riveted beam-column connection of the Syndicate building was analyzed using finite element software ANSYS V17.2. The results obtained from the analysis are plotted in the previous chapter, which shows that the load carrying capacity and the moment capacity of the connection was improved due to the use of FRP.



The load carrying capacity and the moment capacity of the retrofitted specimen is calculated to be significantly larger than the non-retrofitted specimen when the column was axially loaded in positive Z direction. The increment in load carrying and moment capacity up to 40% more than the non-retrofitted connection (calculated in Chapter V) corroborates the claim made in previous sentence. However, the effect of retrofitting when the loading is applied in negative Z direction looks minor. Since the basic history of earthquake load is like the cycling loading consisting of one or more cycle of positive and negative loading, the magnitude of the peak load deformation and peak moment capacity obtained from loading the column in negative Z direction should be considered when performing a retrofitting design and analysis.

In summary, it can be concluded that the FRP retrofitting has affected the behavior of the connection of the concrete encased beam-column connection knowingly in both the direction of loading. The results indicate that the FRP retrofitting technique used in the research has increased the load, displacement and moment carrying capacity of the connection, owing to slightly better performance of the connection.

## REFERENCES

- ACI Committee 318. Building Code Requirements for Structural Concrete: (ACI 318-14); and Commentary (ACI 318R-14). American Concrete Institute, 2014.
- American Society of Civil Engineers (2017) ASCE Standard ASCE/SEI 41-17: Seismic Evaluation and Retrofit of Existing Buildings, 2017 Edition, ASCE, Virginia
- American Institute of Steel Construction, Seismic Design Manual, 3<sup>rd</sup> Edition
- ANSYS (2017), Swanson Analysis Systems Inc.
- ATC-24. (1992), Guidelines for Cyclic Seismic Testing of Components of Steel Structures, *Applied Technical Council*
- Azarm, R., Maheri, M. R., and Torabi, A. (2016). "Retrofitting RC Joints Using Flange-Bonded FRP Sheets."
- Bisson, M. A. (1997). "An Experimental Study on the Cyclic Behavior of Riveted Stiffened Seat Angle Connection with Concrete Encasement", *Thesis Ottawa-Carleton Institute for Civil Engineering*
- Ghobarah, A., and Said, A. (2001). "Shear Strengthening of beam-column joints."
- Ghobarah, A., Aziz, T. S, and Biddah, A. (1997). "Rehabilitation of reinforced concrete frame connections using corrugated steel jacketing." *ACI Structural Journal*
- Ghobarah, A., Biddah, A., and Mahgoub, M. (1997). "Seismic Retrofit of reinforced concrete columns using steel jackets." *European Earthquake Engineering*
- Hany, N. F., Hantouche, E. G., and Harajli, M. H. (2016). "Finite element modeling of FRP-confined concrete using modified concrete damaged plasticity."
- Hosseini, F., Gencturk, B., Aryan, H., and Cadaval, G. (2018). "Seismic behavior of 3-D ECC beam-column connections subjected to bidirectional bending and torsion."
- Ibrahim, A. M., and Mahmood, M. S. (2009). "Finite element modeling of reinforced concrete beams strengthened with FRP laminates."
- Imam, B. M., Righiniotis, T. D., and Chryssanthopoulos, M. K. (2007). "Numerical Modelling of Riveted Railway Bridge Connections for Fatigue Evaluation" *University of Surrey, United Kingdom*

- Karimi, K., El-Dakhakhni, W. W., and Tait M. J. (2012). "Behavior of Slender Steel-Concrete Composite Columns wrapped with FRP jackets."
- Karimi, K., El-Dakhakhni, W. W., and Tait, M. J. (2011). "Performance Enhancement of Steel Columns using concrete-filled composite jackets."
- Karimi, K., Tait, M. J., and El-Dakhakhni, W. W. (2009). "A novel retrofit technique for strengthening steel columns using FRP."
- Le-Trung, K., Lee, K., Lee, J., Lee, D. H., and Woo, S. (2009). "Experimental study of RC beam-column joints strengthened using CFRP composites."
- MacGregor, J.G. (1992). "Reinforced Concrete Mechanics and Design, Prentice-Hall, Inc., Englewood Cliffs N.J."
- Masuelli, M. A. (2013). "Introduction of Fibre-Reinforced Polymers – Polymers and Composites: Concepts, Properties and Processes."
- Mostofinejad, D., Akhlaghi, A., and Eslami, A. (2017). "Estimating the Seismic Performance of CFRP-Retrofitted RC Beam-Column Connections Using Fiber-Section Analysis." *Journal of Earthquake Engineering*
- Naderi, M. (2008). "Finite element analysis of riveted joints in old steel buildings in NZ" *NZSEE Conference 2008*
- Pantelides, C. P., Okahashi, Y., and Reaveley, L. D. (2008). "Seismic Rehabilitation of Reinforced Concrete Frame Interior Beam-Column Joints with FRP Composites."
- Pavan, K. D. V. T. G., Naarayan, S. S., Sundaram, K.S., and Chandra, S. (2011). "Further numerical and experimental failure studies on single and multi-row riveted lap joints"
- Qudah, S., and Maalej, M. (2014). "Application of engineered cementitious composites (ECC) in interior beam-column connections for enhanced seismic resistance."
- Rocchi, J. (2015). "Six Practical Reasons to save Old Buildings", <https://savingplaces.org/stories/six-reasons-save-old-buildings#.XDy9AVxKiM8> (Jan. 14, 2019)
- Rodrigues, M. P. G., Jesus, A. M. P., and Silva, A. L. L (2010). "Comparison between alternative FE modeling strategies for riveted connections concerning fatigue assessments"
- Shanmuganathan, S., and Clifton, C. (2004). "Evaluation of Seismic Resistance of existing moment resisting steel frame buildings"
- Steel Design Guide 6. (1992), Load and Resistance Factor Design of W-Shapes Encased in Concrete

Wikipedia. “Fibre-reinforced plastic”, <[https://en.wikipedia.org/wiki/Fibre-reinforced\\_plastic](https://en.wikipedia.org/wiki/Fibre-reinforced_plastic)> (Jan. 14, 2019)

Wikipedia. “The Syndicate (building)”, <[https://en.wikipedia.org/wiki/The\\_Syndicate\\_\(building\)](https://en.wikipedia.org/wiki/The_Syndicate_(building))> (Jan. 13, 2019)

Wu, Y., Liu, T., and Oehlers, D. J. (2006). “Fundamental Principles that govern Retrofitting of Reinforced Concrete Columns by Steel and FRP Jacketing.”